iScience

CellPress
OPEN ACCESS

Article

Mapping structural distribution and gating-property impacts of disease-associated mutations in voltage-gated sodium channels

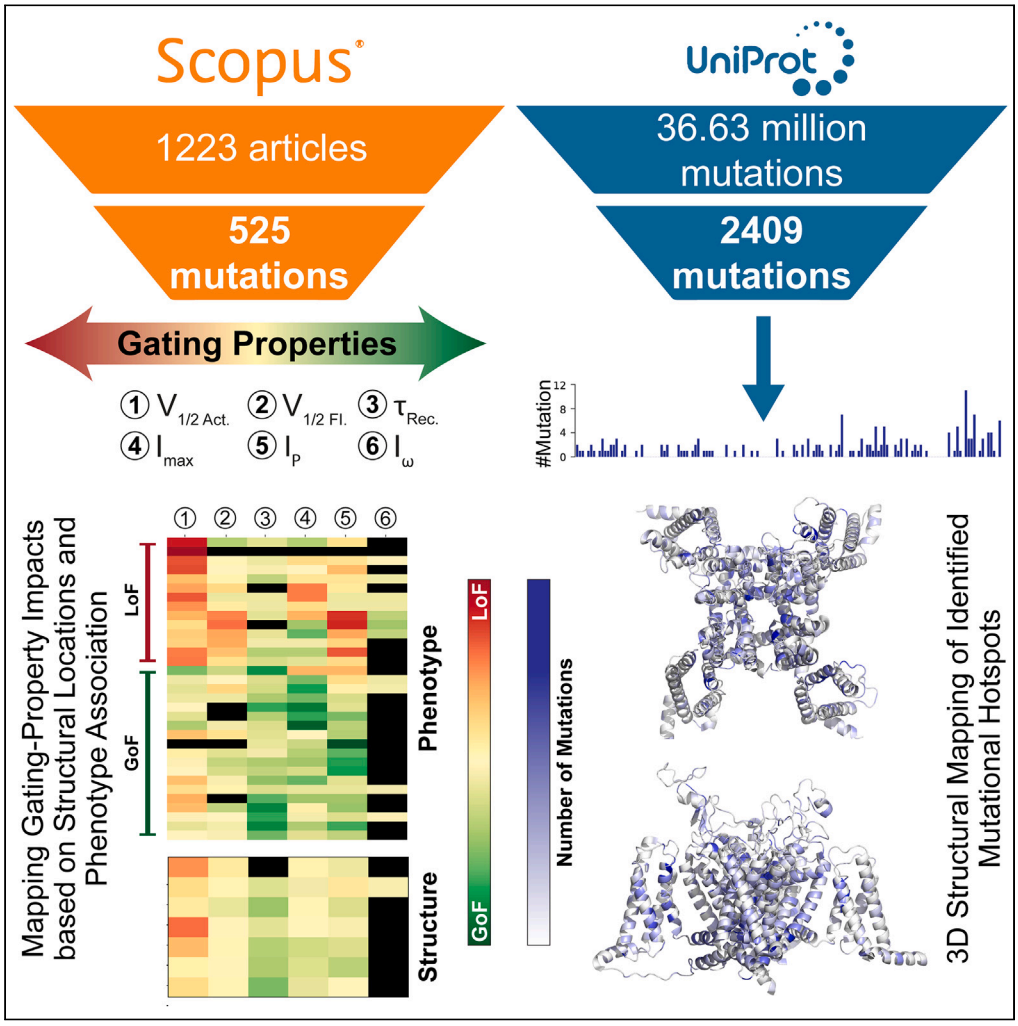

Amin Akbari Ahangar, Eslam Elhanafy, Hayden Blanton, Jing Li

jli15@olemiss.edu

Highlights

Mapped 2,400 mutations in Na_v channels and identified clusters of mutation hotspot

Mapped gating-property impacts of 525 mutations from 366 electrophysiology studies

Revealed gating property is vital for precisely predicting variant effects in Na_v

Identified patterns of gating-property impacts for key structural regions

Akbari Ahangar et al., iScience 27, 110678
September 20, 2024
https://doi.org/10.1016/j.isci.2024.110678

iScience

CellPress
OPEN ACCESS

Article

Mapping structural distribution and gating-property impacts of disease-associated mutations in voltage-gated sodium channels

Amin Akbari Ahangar,[1] Eslam Elhanafy,[1] Hayden Blanton,[1] and Jing Li[1,2,*]

SUMMARY

Thousands of voltage-gated sodium (Na_v) channel variants contribute to a variety of disorders, including epilepsy, cardiac arrhythmia, and pain disorders. Yet, the effects of more variants remain unclear. The conventional gain-of-function (GoF) or loss-of-function (LoF) classifications are frequently employed to interpret mutations' effects and guide therapy for sodium channelopathies. Our study challenges this binary classification by analyzing 525 mutations associated with 34 diseases across 366 electrophysiology studies, revealing that diseases with similar GoF/LoF effects can stem from unique molecular mechanisms. Utilizing UniProt data, we mapped over 2,400 disease-associated missense mutations across Na_v channels. This analysis pinpoints key mutation hotspots and maps patterns of gating-property impacts for the mutations, respectively, located around the selectivity filter, activation gate, fast inactivation region, and voltage-sensing domains. This study shows great potential to enhance prediction accuracy for mutational effects based on the structural context, paving the way for targeted drug design in precision medicine.

INTRODUCTION

Bioelectrical signals, responsible for phenomena such as heartbeats, muscle contractions, and rapid cognitive processing, hinge on the function of ion channels.[1] Among these, voltage-gated sodium (Na_v) channels are particularly prevalent, playing a crucial role in initiating action potentials and underpinning electrical excitability.[2] Progress in gene research and functional assays has led to the identification of thousands of Na_v channel mutations associated with a range of excitability disorders affecting the heart, muscles, and brain.[3–7] For instance, the $Na_v1.5$ channel, primarily associated with cardiac function, has been linked to an array of inherited arrhythmias due to a multitude of natural variants.[8,9] Similarly, various forms of periodic paralysis are caused by mutations in the $Na_v1.4$ channel, which is primarily found in skeletal muscles.[7,10] In the realm of neurological disorders, mutations in the $Na_v1.1$, $Na_v1.2$, $Na_v1.3$, and $Na_v1.6$ channels, predominantly located in the brain, have been tied to genetic epilepsy, autism, migraines, and other neurological conditions.[7,11] Lastly, dysfunction of the $Na_v1.7$ channel, largely situated in peripheral neurons, is implicated in a wide range of pain disorders.[12,13]

Pathogenic mutations can disrupt the standard function of Na_v channels by either amplifying (gain-of-function, or GoF) or diminishing (loss-of-function, or LoF) Na^+ current.[14] These opposite effects on channel function can result in a spectrum of disorders.[7,15] For example, GoF mutations in the $Na_v1.5$ channel can trigger long QT syndrome type 3 (LQT3), while LoF mutations in the same channel have been linked to various conditions, such as Brugada syndrome (BRGDA1) and dilated cardiomyopathy (DCM).[8,9] Similarly, GoF missense mutations in the $Na_v1.7$ channel have been found to induce primary erythermalgia (PEM) and paroxysmal extreme pain disorder (PEPD), while LoF mutations result in an insensitivity to pain.[12] Likewise, GoF variants in the $Na_v1.2$ channel have been associated with conditions like infantile epileptic encephalopathy and benign familial infantile seizures (BFIS3), whereas LoF variants can lead to autism (autism spectrum disorder [ASD]) and/or intellectual disability.[7,16] This genotype-phenotype relationship is similarly observed in other Na_v channels.[7]

The GoF and LoF classifications in Na_v channels have frequently been employed to categorize disease-associated mutations for interpreting genotype-phenotype relationships,[7,15] predicting the functional impact of novel variants,[17,18] and guiding precision therapy[19,20] for sodium channelopathies. Recent studies have explored the correlation between phenotypes and the structural locations of mutations, and have detected the regional clusters and their relationship with overall GoF and LoF phenotype.[17,19] However, several critical questions cannot be addressed by the binary classification of GoF/LoF.

Firstly, the overall gain-of-function (GoF_o) or loss-of-function (LoF_o), which refers to the amplification or reduction of the total sodium current, respectively, does not provide critical details for the nuanced impacts on channel function.[21] Na_v channels undergo three primary steps within their functional cycle: activation, inactivation, and recovery from inactivation.[22] Each of these steps encompasses several gating

[1]Department of Biomolecular Sciences, School of Pharmacy, University of Mississippi, Oxford, MS 38677, USA
[2]Lead contact
*Correspondence: jli15@olemiss.edu
https://doi.org/10.1016/j.isci.2024.110678

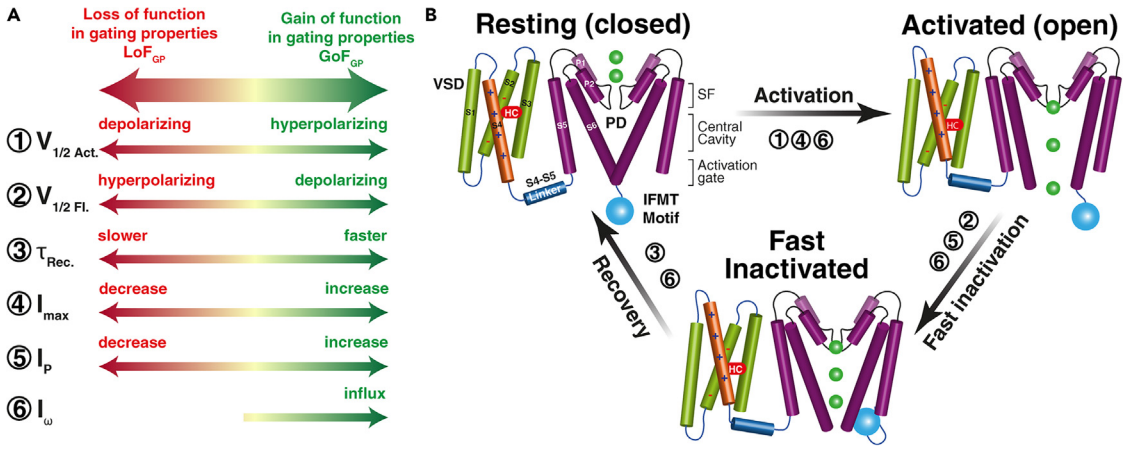

Figure 1. The gating properties and functional transitions of Na$_v$ channels

(A) Gating properties are listed with their GoF$_{GP}$ (green) or LoF$_{GP}$ (red) effects. These properties comprised maximal current amplitude (I_{max}), half-activation voltage in steady-state activation ($V_{1/2\ Act}$), half-inactivation voltage in steady-state fast inactivation ($V_{1/2\ Inact}$), recovery rate (τ_{rec}), persistent current (I_P), and gating pore current (or ω current, I_ω).

(B) The gating properties with their relevant transitions in the functional cycle of Na$_v$ channels. The Na$_v$ structure has four similar subunits (I to IV), and each subunit comprises six transmembrane helices (S1-S6). The first four TMs (S1 to S4) form a voltage-sensing domain (VSD), and the TMs S5 and S6 contribute to the pore domain (PD). Sensing the membrane depolarization, VSDs undergo resting-to-activated structural transition. Then the channel inactivates mediated by allosteric blocking of IFMT motif when depolarization is prolonged to a certain timescale. Thirdly, the repolarization of membrane potential allows recovery from the fast inactivation to the resting state. The gating properties are labeled with their relevant functional step. Please check the supplementary materials for a colorblind-friendly version of this figure.

properties, capable of modifying the Na^+ current at a specific phase (Figure 1B).[2] The alterations in gating properties associated with these steps not only change the total sodium current but also modify the timing and shape of the action potential.[2] Such changes in action potential, for instance in cardiac cells, could lead to differential conditions where the heart beats too fast, too slow, or irregularly.[8,9] These diverse conditions can lead to distinct life-threatening arrhythmias, which cannot be accurately diagnosed or understood solely through the GoF$_o$/LoF$_o$ classification.[21]

Another challenging phenomenon is the occurrence of "overlapping syndromes", where a single mutation can lead to phenotypes with different or even opposing overall effects.[8,23–25] For example, more than 30 mutations in Na$_v$1.5 have been linked to both GoF$_o$-associated LQT3 and LoF$_o$-associated BRGDA1.[23,26] The mystery of how a single point mutation can lead to both GoF$_o$ and LoF$_o$ phenotypes[27,28] adds to the limitations of the conventional GoF$_o$/LoF$_o$ classification system. Understanding these complexities requires a more nuanced examination of Na$_v$ channels and their mutations, going beyond the binary GoF$_o$/LoF$_o$ model.

Moreover, the same phenotype can arise from different gating property changes, mediated by diverse mechanisms.[23,24,29,30] For instance, over 200 LoF$_o$ mutations are associated with BRGDA1, but their functional impacts are mediated through a range of mechanisms, such as the depolarizing shift of activation, hyperpolarizing shift of inactivation, and/or slower recovery from inactivation.[23] This adds another level of complexity to the application of GoF$_o$/LoF$_o$ classification for predicting the mutation's effects and guiding precision therapy.

More importantly, although GoF$_o$/LoF$_o$ classification has provided valuable guidance for therapeutic development and use over the past several decades, it is challenging to further improve the efficacy and accuracy for precision medicine. Given the broad array of mechanisms leading to GoF$_o$/LoF$_o$ effects, developing a universal therapy capable of addressing all similar outcomes is unrealistic, as supported by extensive clinical evidence. For instance, channel blockers are a conventional strategy for treating GoF$_o$ diseases, but numerous reports indicate that Na$_v$ blockers are ineffective for some patients with GoF$_o$ phenotypes.[31,32] Similarly, there is increasing evidence of a lack of response to Na$_v$ blockers in individuals with GoF$_o$ phenotype myotonias.[33,34] In one study, 23 out of 63 (36.5%) myotonia patients showed no improvement with sodium channel blocker treatment.[33] Alternatively, by categorizing mutations based on their impact on gating properties, it may be more promising to design selective drugs targeting groups of mutations that share similar mechanisms. This is why clinicians have started to adjust the medication based on changes in the channel's biophysical properties.[35] Therefore, we propose that therapeutic strategies in the era of precision medicine should not solely target GoF$_o$/LoF$_o$ effects, but rather focus on correcting the altered gating properties induced by mutations.

In the current study, a large-scale analysis is undertaken, leveraging the most recent electrophysiological and genetic data to map the distribution of mutations and identify common patterns of mutational effects on gating properties. Firstly, a large number of research articles have measured the mutational effects on different gating properties over the past three decades. To synthesize this wealth of knowledge on variant effects, we conducted a meta-analysis of 366 independent studies on missense mutations based on human cell lines. A systematic literature search was performed to gather the gating properties of 525 mutations from previous electrophysiological measurements (Figure 2A). This meta-analysis enables us to compare homologous mutations across different channels and group mutations or phenotypes

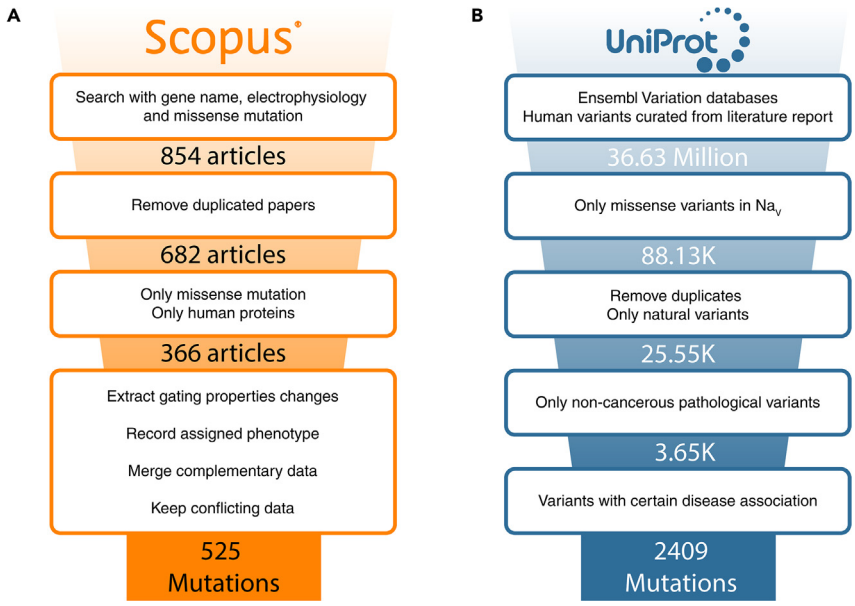

Figure 2. The workflow in the study for collecting electrophysiology and genetic data

(A) The workflow to search and extract electrophysiology research articles that study the mutational effects on gating properties. A total of 854 articles from Scopus were reviewed, and a rigorous selection process identified 366 articles relevant to this study. From these articles, 525 unique mutations with gating properties were identified and selected as the core data for further analysis and investigations.

(B) Data extraction steps to retrieve disease and variant data from UniProt. Initially, more than 36 million mutations in UniProt were filtered, resulting in a refined dataset of 2.4K non-cancerous pathogenic missense mutations in Na_v.

based on alterations in gating properties (Figure 3), providing deeper insights into the fundamental principles underlying the disturbed biophysical impacts induced by various mutations. Furthermore, approximately 2,400 annotated disease-associated missense mutations of the nine human Na_v channels from the UniProt database (Figure 2B) to equivalent positions are mapped into structural segments (Figure 4) and the multiple sequence alignment (MSA) (Figure 5). We can map mutation distributions (Figures 6 and 7), identify the most representative mutations with conserved functional significance (Table S1), and, crucially, explore the way to predict mutational effects based on their structural location and context.

RESULTS

Mapping the gating-property impacts of sodium channelopathies

We carried out an exhaustive literature search across Scopus, yielding 854 papers that reported electrophysiology measurements of gating properties for Na_v channel mutants. Duplicate research articles were eliminated, and the records lacking a patch-clamp experiment on a pathogenic missense mutation of human Na_v channels were excluded (Figure 2). Following this, we performed a thorough full-text analysis on 366 articles, documenting 525 variants and their influence on several crucial gating properties. These properties comprised maximal current amplitude (I_{max}), half-activation voltage in steady-state activation ($V_{1/2\ Act}$), half-inactivation voltage in steady-state fast inactivation ($V_{1/2\ Inact}$), recovery rate (τ_{rec}), persistent current (I_P), and gating pore current (or ω current, I_ω) (Figure 1). We recognize that protein expression, folding, trafficking, and post-translational modifications (PTMs) are also essential properties that can be influenced by mutations. Therefore, some of these properties are documented in Table S3. Often, such impacts can affect the peak current amplitude (I_{max}), even if they do not directly alter the protein structure. Our review indicates that protein expression, folding, and trafficking are less frequently reported in electrophysiology studies compared to the gating properties (refer to Table S3). Due to the limited availability of relevant data, these properties are not explicitly included in our analysis.

In this study, we recognize that alterations in each gating property in all electrophysiology measurements lead to amplification or reduction of the Na^+ current at specific steps in the functional cycle. To effectively summarize the mutational effects on each gating property from 366 research articles, we have categorized the impacts on each gating property based on gain-of-function or loss-of-function, referred to as GoF_{GP} (gain of function on a gating property) and LoF_{GP} (loss of function on a gating property), respectively (Figure 1). This terminology helps to distinguish the effects on individual gating properties from the overall gain-of-function (GoF_o) or loss-of-function (LoF_o) effects on Na_v channels. This distinction is crucial as it provides a more nuanced understanding of how mutations affect Na_v channel function at specific stages, further aiding in understanding mutation impacts more precisely.

To categorize the sodium channelopathies and compare their gating-property impacts, a GoF_o/LoF_o categorization was applied to 34 diseases across the nine Na_v channels based on overall effects in previous literature (Table S2). In order for a disease to be included in

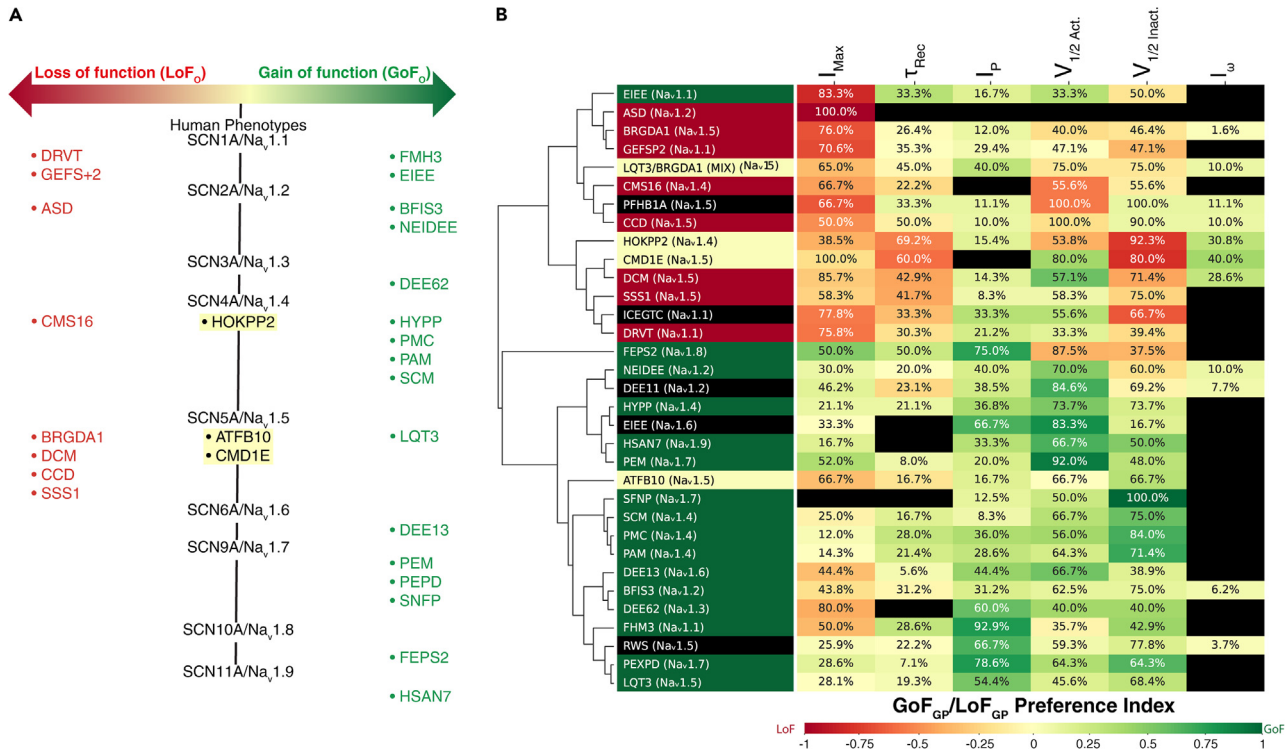

Figure 3. The classification of Na$_v$ associated diseases based on overall mutational effect or impacts on gating properties

(A) 34 sodium channelopathies are grouped based on a binary GOF$_o$/LOF$_o$ classification according to previous literature (Table S2). Diseases are colored in green for GoF$_o$ phenotypes, red for LoF$_o$ phenotypes, and yellow for diseases with mixed overall effect (MIX$_o$).

(B) Gating-property impacts of 536 mutations are mapped into their associated 34 diseases. The diseases are also clustered based on the similarity of the gating-property impacts of their associated mutations. The GoF$_{GP}$/LoF$_{GP}$ preference index is depicted colorimetrically with dark green representing highly consistent GoF$_{GP}$ effect, dark red for highly consistent LoF$_{GP}$ effect, and black no such a gating-property data available. The percentage (%) of mutations affecting a certain gating property within a specific phenotype is shown in each grid. Please check the supplementary materials for a colorblind-friendly version of this figure.

this analysis, it had to have at least five associated mutants that were reported in previous electrophysiological studies (Table S3). Based on previous literature (Table S2), eight diseases were associated with inferred LoF$_o$ effect, eighteen were associated with inferred GoF$_o$ effect, three were suggested to have mixed effects, and the effects of five diseases remain unclear (See Figure 3A). Considering the fact that many mutants in Na$_v$1.5 are associated with both LQT3 and BRGDA1, these mutants were exclusively grouped for a mixed phenotype (LQT3/BRGDA1). The mixed phenotype categorization highlights the complex relationships between specific mutations, channel functionality, and resulting diseases.

Sodium channelopathies, as identified in our analysis (Figure 3B), cluster into two primary branches based on their altered gating properties, predominantly aligning with the GoF$_o$/LoF$_o$ categorization. EIEE(Na$_v$1.1) is the sole GoF$_o$ phenotype grouped with most LoF$_o$ diseases (Figure 3B), yet the overall effect of EIEE(Na$_v$1.1) remains a subject of ongoing debate.[7]

However, within each of these branches, there are diseases with significant differences in their altered gating properties. This observation implies that diseases with similar overall effects (either GoF$_o$ or LoF$_o$) are triggered by distinctive molecular mechanisms. For instance, among GoF$_o$ phenotypes, both familial episodic pain syndrome 2 (FEPS2, associated with Na$_v$1.8) and benign familial infantile 3 (BFIS3, associated with Na$_v$1.2) belong to this branch. However, their variant effects on several gating properties are almost opposite: a large portion of FEPS2 mutations increase I$_{max}$, speed up recovery, depolarizing shift V$_{1/2\ Act}$, and hyperpolarizing shift V$_{1/2\ Inact}$, whereas similar proportions of BFIS3 mutations decrease I$_{max}$, slow down recovery, hyperpolarizing shift V$_{1/2\ Act}$, and depolarizing shift V$_{1/2\ Inact}$ (Figure 3B). This clear distinction suggests that these two pain disorders are driven by entirely different mechanisms, and as a result, their treatments for restoring normal channel function should also be unique. A similar divergence is observed within the LoF$_o$ branch, DCM (associated with Na$_v$1.5) mutations cause hyperpolarizing shift of V$_{1/2\ Act}$, hyperpolarizing shift V$_{1/2\ Inact}$, or slow τ_{rec}. In contrast, most PFHB1A (associated with Na$_v$1.5) mutations cause a depolarizing shift of V$_{1/2\ Act}$, lead depolarizing shift of V$_{1/2\ Inact}$, or speed up τ_{rec}. Given that a large portion of mutations associated with these two diseases affect these three gating properties, it is clear that these two diseases, despite having a LoF$_o$ effect, must be driven by distinct mechanisms.

Our analysis shows that the same overall effect (either GoF$_o$ or LoF$_o$) can be caused by differential influences on different gating properties. This implies that certain gating properties might have a dominant role in shaping the overall effect, even when other gating properties are

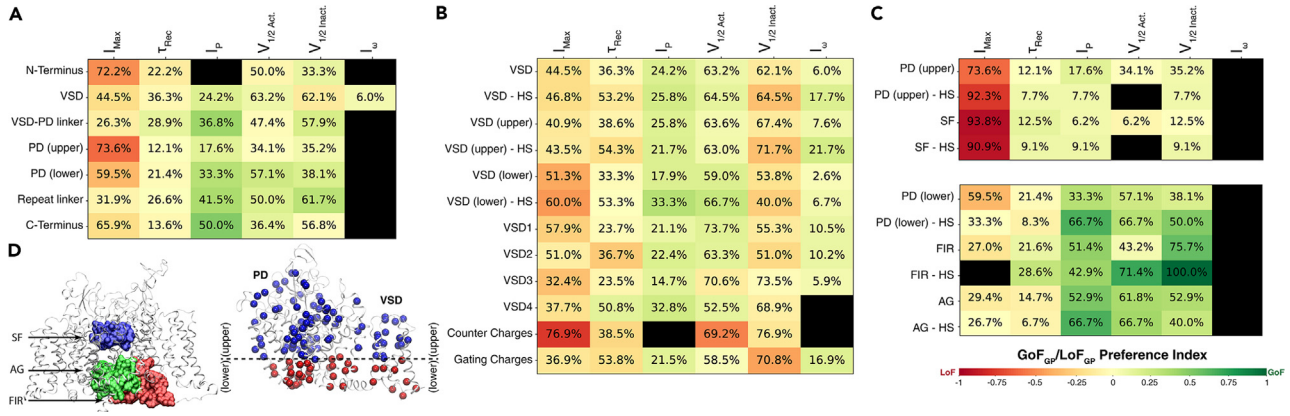

Figure 4. Preferences of gating-property impacts for disease-associated mutations in different structural segments

The variant effects on six gating properties of 525 mutations from 366 papers are mapped into seven major structural segments (A), different selections in VSDs (B), and PD (C). HS stands for the mutation hotspots of corresponding structural segments. The percentage (%) of mutations affecting a certain gating property within a specific structural segment is shown in each grid. GoF_{GP}/LoF_{GP} preference index is depicted colorimetrically with dark green representing highly consistent GoF_{GP} effect, dark red for highly consistent LoF_{GP} effect, and black for no such gating-property data available.

(D) Shows the selection for selectivity filter (SF), activation gate (AG), fast inactivation region (FIR), as well as the upper and lower part for PD and VSD. The disease-associated mutations are represented in blue (upper) and red (lower) spheres. Please check the supplementary materials for a colorblind-friendly version of this figure.

influenced in an opposite manner. For instance, in DEE13 (Nav1.6), 66.7% of mutations lead to a shift in the $V_{1/2\ Act}$, with the majority trending toward a hyperpolarizing direction, producing a GoF_{GP} effect. At the same time, 44.4% of DEE13 mutations alter I_{max}, with most reducing I_{max}, resulting in a LoF_{GP} effect (Figure 3B). These two gating property changes are diametrically opposite, yet the net effect is categorized as GoF_o. While in FEPS2 ($Na_v1.8$), the mutations that alter $V_{1/2\ Act}$ and $V_{1/2\ Inact}$ lead to a LoF effect. However, a more dominant GoF effect is brought about by stronger impacts on the maximum ionic current (I_{max}) and persistent current (I_P) (Figure 3B). Similarly, in dilated cardiomyopathy 1E (CMD1E, $Na_v1.5$), 80% of associated mutations prefer a hyperpolarizing shift of $V_{1/2\ Inact}$ and 60% of these mutations tend to slow the recovery time constant (τ_{rec}). Although the mutational impact on the $V_{1/2\ act}$ is $GoF_{GP,}$ the alterations on $V_{1/2\ Inact}$ and τ_{rec} together bring about a LoF_o effect. In PFHB1A ($Na_v1.5$), most associated mutations decrease I_{max} and cause a depolarizing shift of $V_{1/2\ Act}$, leading to the LoF_o effect, despite their GoF_{GP} effects on $V_{1/2\ Inact}$. In summary, the overall effect of a disease is not solely determined by the direction (either GoF_{GP} or LoF_{GP}) of individual variant effects on gating properties. Instead, it is the cumulative effect of these alterations, with some gating properties potentially playing a more dominant role than others in determining the overall effect. Such cumulative effects of variant influences on gating properties are in line with established mathematical models, such as the single-compartment conductance-based model.[36] This model, which incorporates detailed voltage-clamp data to predict neuronal excitability, has been effectively used to correlate electrophysiological scores with clinical severity in SCN8A variants.[37,38]

An additional pattern observed in our analysis is that almost all LoF_o diseases show mixed effects on different gating properties (Figure 3B). For instance, BRGDA1($Na_v1.5$) demonstrates not only a robust LoF_{GP} impact on I_{max}, and moderate LoF_{GP} effects on $V_{1/2\ Act}$, $V_{1/2\ Inact}$, and τ_{rec}, but also GoF_{GP} impacts on I_P and I_ω. This is likely due to the fact that, as observed in electrophysiological measurements, impacts on I_P and I_ω mostly prefer to be GoF_{GP} for all phenotypes (Figure 3B). However, even when I_P and I_ω are excluded, many LoF_o diseases, such as DRVT($Na_v1.1$), ICEGTC ($Na_v1.1$), DCM($Na_v1.5$), PHFB1A($Na_v1.5$), CCD($Na_v1.5$), show opposite impacts on $V_{1/2\ Act}$ and $V_{1/2\ Inact}$. Interestingly, almost all the diseases showing mixed GoF_{GP}/LoF_{GP} effects, including HOKPP2($Na_v1.4$), CMD1E($Na_v1.5$), and LQT3/BRGDA1($Na_v1.5$) are clustered within the LoF_o branch (Figure 3B). This reaffirms that mixed effects are a common feature for diseases within the LoF_o branch. Conversely, although there are several diseases in the GoF_o branch that present mixed effects, more diseases consistently show GoF_{GP} effects on all gating properties (Figure 3B).

In this study, we also compared the variant effects of homologous residues across different Na_v channels, focusing on their biophysical impacts on gating properties and their GoF_o or LoF_o categorizations. Our analysis revealed that the biophysical impacts of mutations in identical residues across different Na_v channels were more likely to align, with 37 out of 44 pairs of identical disease-associated mutations in different Na_v channels resulting in similar alterations in gating properties (Table S4), equating to 86% biophysical agreement. This observation aligns with prior research indicating that analogous positions in Na_v channels may elicit similar biophysical outcomes due to mutations.[19] In contrast, only 60% (74 out of 123) of these mutations showed a consistent GoF_o/LoF_o agreement in their associated diseases (Table S5). There could be multiple reasons for the relatively lower agreement in phenotype classification compared to biophysical impact. Firstly, the predominant gating property influencing the overall effect could vary between different Na_v channels, leading to differential GoF_o/LoF_o effects. For instance, the change in a specific gating property might be amplified due to the interaction between this Na_v channel and other proteins.[39] Secondly, mutations associated with multiple diseases, encompassing both GoF_o and LoF_o phenotypes, might only be partially characterized in terms of their disease associations. Insufficient data could result in these variants being labeled as either GoF_o or LoF_o mutations.

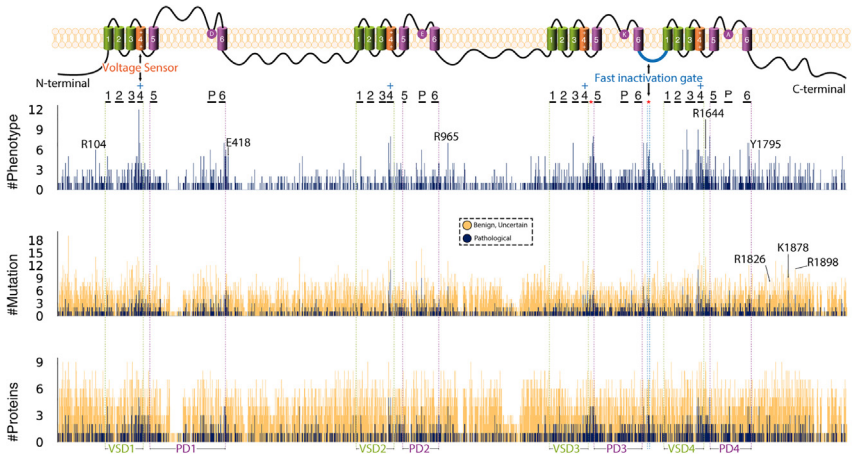

Figure 5. Mapping the mutation hotspots in Na_v channels

The annotated disease-associated mutations from UniProt are mapped to equivalent positions of MSA of the 9 human Na_v channels and the linear protein structure of the channel. The number of phenotypes (upper panel), the number of mutations (middle panel), and the number of proteins with mutation at the same position (lower panel) are used to determine the mutation hotspots. The data for pathogenic missense mutations are shown in blue bars and all information related to all missense (including pathogenic, benign, and uncertain) variants are shown in orange. Hotspots in the N terminal, C terminal, intracellular, and extracellular loops of the proteins are shown in this figure with residue IDs from $Na_v1.5$.

Consequently, predicting the impact of a new variant based on the known biophysical effects of equivalent mutations in other Na_v channels appears to be a more reliable approach than relying on the documented GoF_o/LoF_o classification of the same mutation.

Clustering mutations and their biophysical impacts in 3D structure

The biophysical/functional impact of a mutation should highly depend on its structural role, thus, mapping all disease-associated mutations in Nav channels and their impacts on gating properties in 3D structure would help us to understand and predict the mutational effects of the undocumented variants. The recurrence of mutations across independent samples in disease-associated cases is a robust indicator of functional significance.[40,41] Na_v channels share high sequence, structure, and function similarity.[42] Considering mutations in analogous positions could cause similar biophysical effects in Na_v channels,[17,19] this evolutionarily conserved nature allows us to extrapolate the concept of recurring mutations from a single gene/protein to the Na_v channel family. Based on MSA across nine human Na_v channels, we mapped 2,409 annotated missense mutations from the UniProt database[43] (Figure 2) to their corresponding positions, thus identifying a series of mutation hotspots (Figure 5). These pathogenic mutation hotspots were subsequently visualized within the 3D structure of human $Na_v1.5$ (PDB:7DTC) to display their distribution. Thus, the residues discussed in the following sections are referred to using their residue ID in $Na_v1.5$. Our structural mapping underscores that a significant number of mutation hotspots are predominantly situated within three distinct regions: (1) the voltage-sensing domain (VSD), (2) the upper section of the pore domain (PD [upper])—near the selectivity filter (SF) and pore helices, and (3) the lower part of the pore domain (PD [lower])—including the fast-inactivation segment and activation gate (AG).

In this comprehensive study, we also mapped the effects of known Na_v channel mutations on six gating properties, across respective domains including VSDs, PD (upper), PD (lower), N/C terminals, and additional detailed structural segments (Figure 4). This thorough mapping procedure sheds light on the intricate relationships between the structural locations of mutations and their functional outcomes. While it is evident that mutations within each structural segment can influence most gating properties, no single segment appears to uniformly affect all gating properties in a consistent GoF_{GP} or LoF_{GP} direction. Beyond these general patterns, each structural segment showcases unique traits, displaying differential preferences for specific gating properties or exhibiting characteristic influences on channel behavior. These unique attributes may shape the manifestation of associated diseases. Thus, a detailed understanding of these individual segment features is imperative for gaining insight into disease mechanisms, which could be exploited for the prediction of undocumented mutational effects and the development of targeted therapeutic interventions.

Diverse variant effects in VSDs are highly sensitive to structural context

A major cluster of mutations is located within the VSDs (Figures 4 and 5), critical structural components that sense membrane potential and trigger structural transitions of Na_v channels. Several features characterize the distribution of mutation hotspots within the VSDs. The first distinguishing feature of VSD mutations is their diverse impacts across a wide array of gating properties. Between one-third and two-thirds of these variants affect key properties such as I_{max}, τ_{rec}, $V_{1/2\ Act}$, and $V_{1/2\ Inact}$. As shown in Figure 4A, there is no strong preference between GoF_{GP} and LoF_{GP} effects on these gating properties. In addition, only mutations within VSDs can induce gating pore currents, also termed

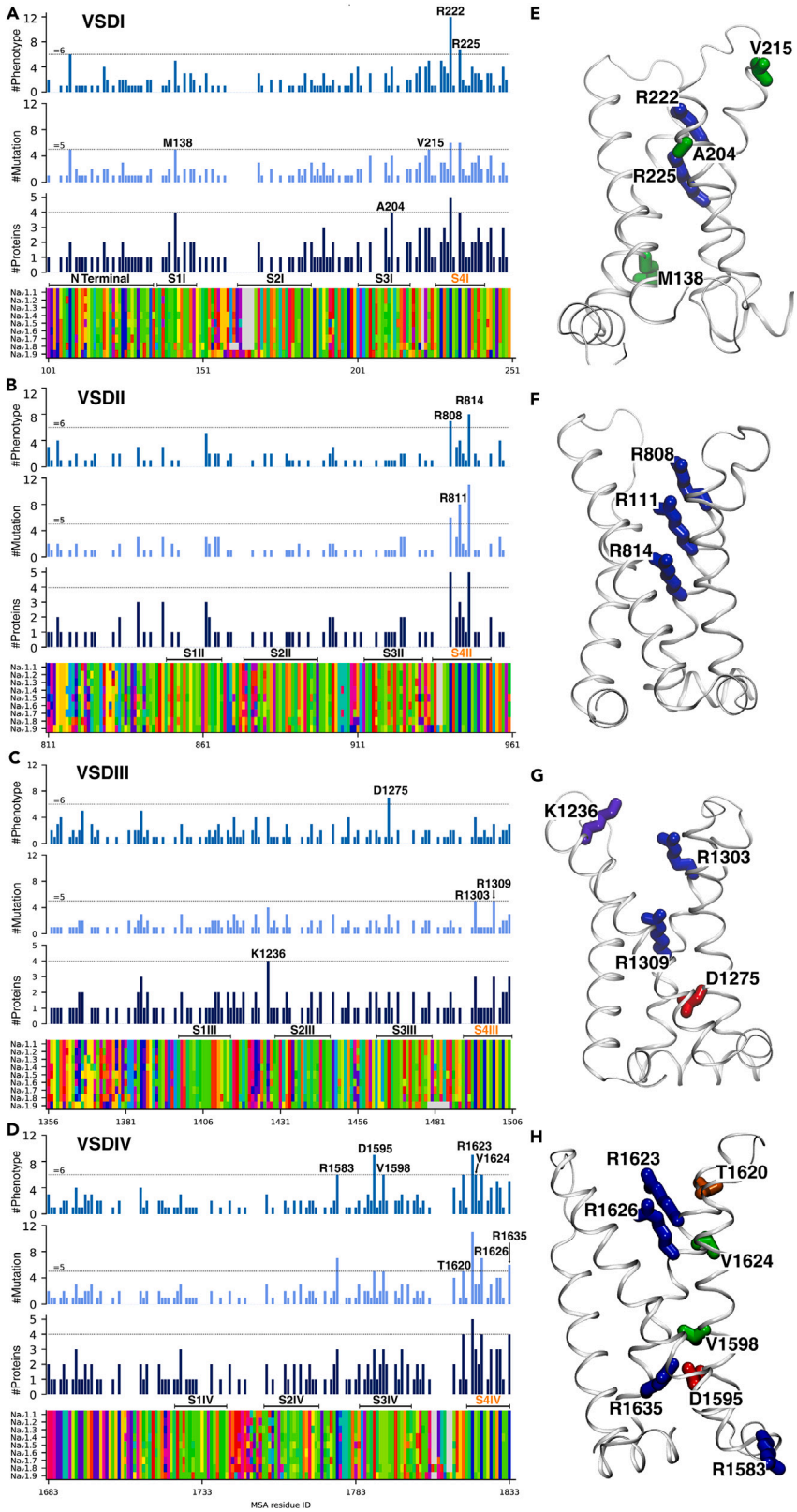
A
VSDI
#Phenotype
#Mutation
#Proteins
R222
R225
M138
V215
A204
N Terminal
S1I
S2I
S3I
S4I
B
VSDII
R814
R808
R811
S1II
S2II
S3II
S4II
C
VSDIII
D1275
R1309
R1303
K1236
S1III
S2III
S3III
S4III
D
VSDIV
D1595
R1623
V1624
R1583
V1598
R1635
R1626
T1620
S1IV
S2IV
S3IV
S4IV
MSA residue ID
E
V215
R222
A204
R225
M138
F
R808
R111
R814
G
K1236
R1303
R1309
D1275
H
R1623
T1620
R1626
V1624
V1598
R1635
D1595
R1583

Figure 6. The mutation hotspots in VSDs

(A–D) The hotspots showing in the MSA of Nav channels for 4 VSDs. All mutation hotspots in VSDs are labeled with the residue IDs in $Na_v1.5$. (E–H) Mapping the hotspots in the structure of VSDs. Residues are shown in licorice and colored according to Taylor color scheme.

omega-pore currents (I_{ω}).[44,45] These currents are produced by protons or cations that pass the channel directly through the VSD.[46–49] Consistently, VSD variants are implicated in most (32 out of 34) sodium channelopathies (Figure 8), each presenting with GoF_o, LoF_o, or mixed GoF_o/LoF_o effect. More intriguingly, some hotspots have been identified as overlap-syndrome mutations that are linked to both GoF_o and LoF_o diseases. For instance, mutations like R222Q, R225W, and R1623Q in $Na_v1.5$ are associated with both LQT3 (GoF_o) and BRGDA1 (LoF_o).[28,50,51] Similarly, R225W in $Na_v1.4$, an equivalent mutation to R225W in $Na_v1.5$, is linked to both congenital myasthenic syndrome (CMS16, LoF_o) and sodium channel myotonia (SCM, GoF_o).[10,52,53]

The second noteworthy feature is the prevalence of mutation hotspots within the S4 helix, specifically gating charges, i.e., R1635 (R5 in VSD_{IV}) (Figure 6D). Na_v channel structures consistently illustrate that the structural transition of VSDs is mediated by the sliding of the S4 helix through the remaining portion of this domain (Figure 1B).[22,54–56] Arrayed along the S4 helix across the membrane, four to six gating charges (arginine or lysine) named R1 to R6 from the extracellular to intracellular side, serve as the voltage sensors in VSDs. Our hotspot analysis indicates that mutations of gating charges tend to recur more frequently in diseases compared to non-gating charge mutations, thereby affirming their functional significance. Interestingly, these mutation hotspots are predominantly distributed in R1 to R3, including R808 (R1 in VSD_{II}), R1303 (R1 in VSD_{III}), R1623 (R1 in VSD_{IV}), R222 (R2 in VSD_I), R811 (R2 in VSD_{II}), R1626 (R2 in VSD_{IV}), R225 (R3 in VSD_I), R814 (R3 in VSD_{II}), and R1309 (R3 in VSD_{III}) (Figure 6). In contrast, fewer hotspots are observed in the gating charges near the intracellular side, with only one hotspot in R5 (R1635 in VSD_{IV}) and no hotspot in R4 in any VSD. Additionally, several conserved countercharge residues, like D1274 (VSD_{III}) and D1595 (VSD_{IV}), are also identified within mutation hotspots. As these countercharges form salt bridges with gating charges, they also contribute to voltage dependence and structural transition.[57] However, hotspots in countercharges are considerably fewer than those in gating charges, and most countercharge hotspots are situated at the intracellular negatively charged region (INC) (Figure 6).

Similar to all variants in VSDs, mutations of gating charges yield diverse effects on a variety of gating properties. Statistically, these gating-charge mutations show only a moderate preference toward LoF_{GP} on I_{max}, τ_{rec}, $V_{1/2\ Act}$, $V_{1/2\ Inact}$, and I_P. Notably, gating-charge mutations are the primary variants that lead to gating-pore currents (I_{ω}), which more frequently bring a GoF_{GP} effect in Na_v channels at the molecular level. These mutations, which lead to the gating-pore current, represent clinically distinct entities that were previously termed "S4 disorders".[58] These mutations provide quintessential examples that the impacts of mutations are strongly influenced by the structural context. For instance, mutations of R2 in VSD_I and VSD_{II} can lead to diverse impacts due to the unique interactions within each VSD. Specifically, R2 mutations in VSD_I are likely to result in a hyperpolarizing shift in $V_{1/2\ Act.}$ and $V_{1/2\ InAct.}$,[48,59] or increasing the maximum sodium current.[48] Conversely, the same mutations in VSD_{II} can cause a depolarizing shift in $V_{1/2\ Act.}$, a hyperpolarizing shift in $V_{1/2\ InAct.}$, and a reduction in both maximum current amplitude and persistent current.[60–62] It is important to note that studies on R2 mutations in VSD_I have reported mixed effects from these mutations,[63–66] indicating varying outcomes. However, mutations in VSD_{II} consistently exhibit a clear LoF_o effect. As such, predicting the effects of a gating-charge mutation remains a challenging task, given that the effects are highly sensitive to nearby residues in different structural states.

The third feature lies in the non-uniform distribution of mutation hotspots across the four VSDs. Specifically, VSD_{IV} hosts more mutation hotspots compared to the other three VSDs. These hotspots encompass the gating charges (R1623, R1626, R1635), countercharge (D1595), a positively charged residue in the S2-3 loop (R1583), as well as neutral residues (V1598, T1620, V1624) (Figure 6). Prior studies have illustrated that the initial three VSDs collectively activate the channel, while VSD_{IV} serves as the critical determinant for both the onset of fast inactivation and recovery.[67–69] The unique functional roles of the VSDs could potentially explain the disparity in the distribution of hotspots. VSD_{IV}, in particular, plays a pivotal and distinctive role, mirroring its higher concentration of mutation hotspots. This functional variation among the VSDs is further reflected in their impacts on gating properties. For VSD_I and VSD_{II}, there are more mutations influencing the $V_{1/2\ Act}$ than $V_{1/2\ Inact}$. Conversely, more mutations in VSD_{IV} affect $V_{1/2\ Inact}$ than $V_{1/2\ Act}$. In addition, more mutations in VSD_{IV} impact the recovery rate (τ_{rec}) than do those in VSD_I to VSD_{III} (Figure 4).

Most mutations reduce ion conductivity in the upper pore domain

Being the pivotal structure of Na_v channels, the PD governs the permeation of Na^+ ions via three key functional transitions: activation, inactivation, and recovery.[22] Thus, it is reasonable that our disease-associated mutation map identifies an abundance of mutation hotspots in the PD. These hotspots are predominantly concentrated in two areas: the upper (PD [upper]) and lower (PD [lower]) parts of the PD.

Within the PD (upper), mutations are widespread in regions such as S5, S6, pore helices, pore loops, and extracellular loops (Figure 7). However, the majority of the mutation hotspots are found in structural segments proximate to the SF, including pore helices (L1 and L2) and the pore loop (Figure 7). Apart from a few non-charged residues (P1438 [$L2_{III}$], G1712 [$P1_{IV}$], and C1728[$L2_{IV}$]), most hotspots in this region are charged residues such as R367 ($P1_I$), R383 ($L2_I$), R878 ($L1_{II}$), R893 ($P1_{II}$), E901 ($P1_{II}$), and D1741($L2_{IV}$). Pathogenic effects invariably ensue from mutations of these charged residues. For example, mutations such as R878C, R893C, and E901K in $Na_v1.5$ all induce BRGDA1,[28,70] while R367C ($P1_I$) exhibits mixed effects, being associated with both LQT3 and BRGDA1.[28,50,71,72]

Contrary to VSD mutations, mutations in the PD (upper) region demonstrate greater consistency in their impacts on gating properties. 93.8% of mutations located near the SF affect I_{max} and most of them result in reduced I_{max} of Na_v channels, and only approximately 10% of mutations affect other gating properties such as τ_{rec}, I_P, $V_{1/2\ Act}$, and $V_{1/2\ Inact}$ (Figure 4). Our hypothesis is that these mutations disrupt

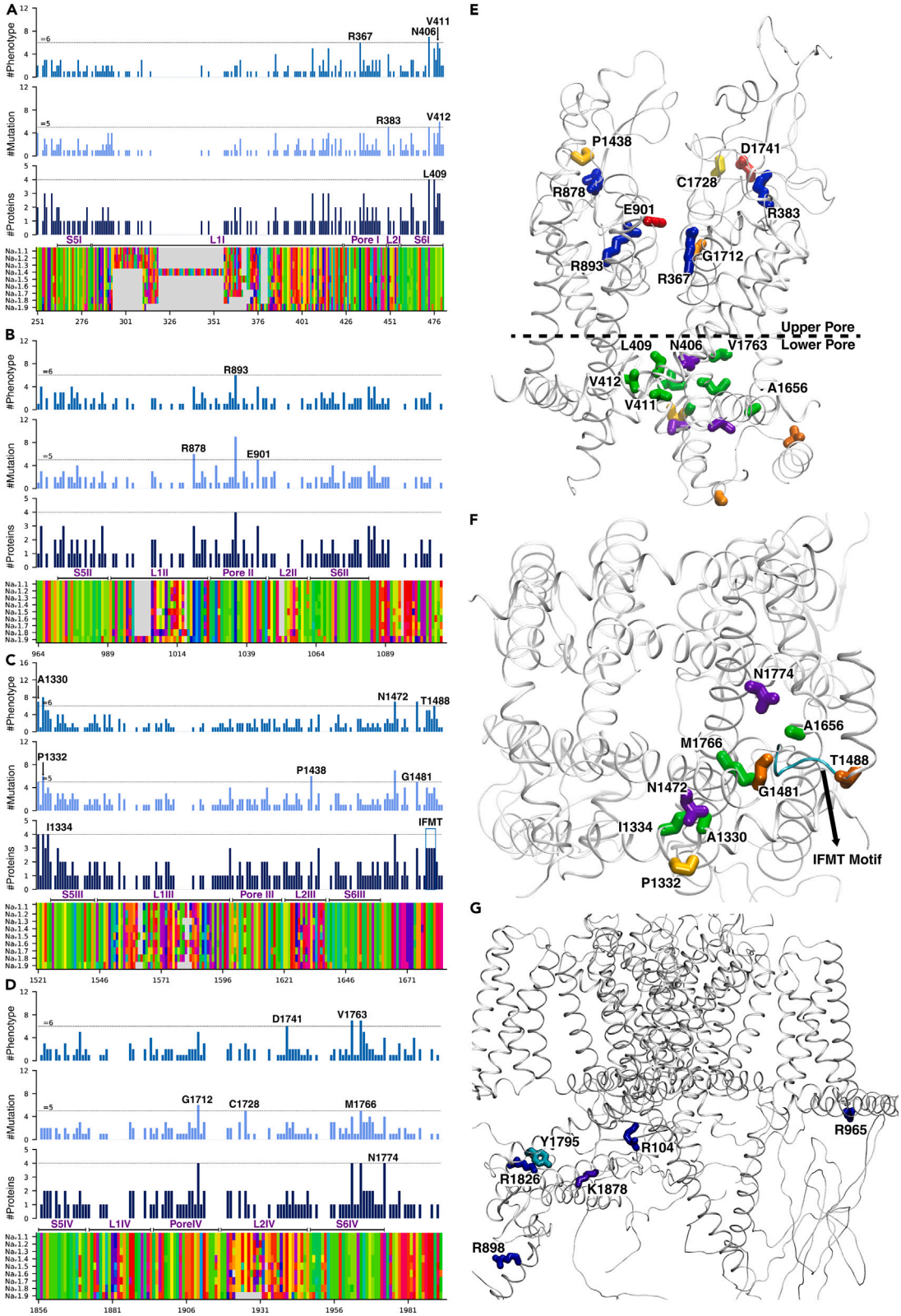
A
#Phenotype
R367
V411
N406
#Mutation
R383
V412
#Proteins
L409
S5I
L1I
Pore I
L2I
S6I
B
R893
R878
E901
S5II
L1II
Pore II
L2II
S6II
C
A1330
N1472
T1488
P1332
P1438
G1481
I1334
IFMT
S5III
L1III
Pore III
L2III
S6III
D
D1741
V1763
G1712
C1728
M1766
N1774
S5IV
L1IV
PoreIV
L2IV
S6IV
E
P1438
D1741
C1728
R878
E901
R383
G1712
R893
R367
Upper Pore
L409
N406
V1763
Lower Pore
V412
A1656
V411
F
N1774
A1656
M1766
T1488
G1481
N1472
I1334
A1330
IFMT Motif
P1332
G
R965
Y1795
R104
R1826
K1878
R898

Figure 7. The mutation hotspots in the pore domain

(A–D) The hotspots in PD showing in the MSA of Na_v channels. (E–G) Mapping of the hotspots in the PD of the $Na_v1.5$ structure from the sideview (E) and bottom view (F). The mutation hotspots at the intracellular loops are shown in the right bottom image (G).

critical interactions adjacent to the SF, such as salt bridges, potentially causing conformational changes to the SF and altering ion permeability. For instance, R893 directly forms salt bridges with two glutamate residues, E898 (SF_{II}) and E901 ($P2_{II}$). Notably, both R893C and E901K have been associated with BRGDA1.[28] Similarly, R878 forms a salt bridge with D1430 ($P2_{III}$) from the neighboring repeat. It's noteworthy that the probability of mutations impacting I_{max} in the entire PD (upper) decreases to 73.6%, whereas the mutations affecting $V_{1/2\ Act}$ or $V_{1/2\ Inact}$ increase to one-third (Figure 4C). This suggests that these non-SF mutations affect the structural transitions rather than disrupting the SF conformation. Many of these residues are proximate to the VSD/PD interface, suggesting they likely influence VSD transitions through non-canonical coupling observed in other voltage-gated ion channels.[73]

GoF_{GP} impacts of mutations in the lower pore domain

The PD (lower) contains the AG and encompasses the receptor site of the fast-inactivation IFMT motif situated at the edge of the AG (Figure 1).[74] When mutations occur near the AG or in the fast-inactivation region (FIR), they are primarily associated with GoF_o phenotypes such as LQT3 in $Na_v1.5$[50,75]. The AG, mechanically coupled with the VSDs, responds to the membrane-potential depolarization by opening during activation and subsequently closing during repolarization to revert to the resting state.[22] The hotspot mutations (N406 [S6I], V411 [S6I], V412 [S6I], V1763 [S6IV], M1766 [S6IV], and N1774 [S6IV]) are all situated near the intracellular end (Figure 7), a region critical to the opening and closing of the gate. The mutations of most AG residues are consistently linked with GoF_o phenotypes (Table S2), aligning with our analysis of their effects on gating properties. The majority of these AG mutation hotspots induce a higher persistent current (I_P), hyperpolarize the $V_{1/2\ Act}$, or depolarize the $V_{1/2\ Inact}$ (Figure 4). Accordingly, we propose that these GoF_o mutations may either facilitate the opening of the gate, stabilize the open state, or hinder its complete closure of the gate. Notably, it is observed that some AG mutations can also decrease I_{max}, potentially explaining why a few residues in this region are associated with LoF_o phenotypes.

The fast-inactivation segment, located in the intracellular loop connecting the third and fourth domains (III-IV linker) (Figure 7),[76] is crucial for fast inactivation by binding to its own site at the edge of the AG (Figure 1).[74] The IFMT motif, a triple-hydrophobic motif combined with a polar residue in the III-IV linker (Figure 7), is the essential motif for binding.[77] According to our analysis of mutation hotspots, mutations associated with LQT3 are primarily located in the IFMT motif and its receptor site, with all four amino acids in the IFMT, identified as mutation hotspots (Figure 7). While mutations linked to BRGDA1 or overlap syndromes (both LQT3 and BRGDA1) are also seen among the hotspot mutations, they occur less frequently. For instance, F1486L, M1487L, and T1488R mutations are all associated with LQT3, while I1485V is linked to BRGDA1.[50] The III-IV linker, an elongated loop containing approximately 60 amino acids, also contains mutation hotspots like N1472S and G1481E (Figure 7). Near these residues, additional mutation hotspots can be found in other structural segments, such as the S4-S5III linker, the intracellular ends of S5III and S6III (Figure 7), S4-S5IV linker, and the C-terminal domain (CTD). For example, A1330 from the S4-S5III linker and N1472 from the III-IV linker (Figure 7), both mutation hotspots, are in contact and associated with LQT3.[50] Nearby A1330, residues P1332 and I1334 are also mutation hotspots. I1334V is associated with LQT3,[50] while P1332L is linked to BRGDA1.[28] These residues contribute to fast inactivation by binding the III-IV linker to the PD, thereby allosterically blocking the AG. According to our gating property map, 100% of mutation hotspots in the fast inactivation region (FIR) depolarize $V_{1/2\ Inact}$, thus leading to a GoF_{GP} effect on channel activity. Fewer FIR residues impact the maximal current (I_{max}) compared to AG mutations. Our analysis of variant effects on gating properties confirms that rather than directly blocking the AG, the fast-inactivation segment blocks the gate allosterically. This is consistent with the allosteric blocking mechanism for fast inactivation in Na_v channels.[78,79]

Gating-property impacts of mutations in other structural segments

Although structural segments such as N/C terminals, VSD-PD linkers, and repeat linkers are significantly less conserved than VSDs and PDs, they host a substantial number of disease-associated mutations and exhibit distinct tendencies in their impacts on gating properties. Approximately 60% of mutations located in the VSD-PD linkers and repeat linkers favor a depolarizing shift in $V_{1/2\ Inact}$, a characteristic LoF_{GP} effect. Over one-third of mutations in these linkers also show a strong propensity to increase I_P, another LoF_{GP} effect (Figure 4). These effects mirror those observed in the lower PD, which could be attributed to the fact that these linkers also contribute to fast inactivation. Notably, over 70% of mutations in the N-terminus tend to reduce I_{max} (Figure 4), likely due to the influential role of residues in this region on Na_v channel expression and folding. On the other hand, mutations in the C-terminus have the highest likelihood to increase I_P (Figure 4). Although the structural role of the C-terminus remains largely undeciphered, the observed impacts on gating properties underscore its crucial role in maintaining the channel impermeable in its inactivated and resting states.

The relationship between phenotypes and structural segments

Mapping mutations corresponding to each phenotype onto the structural segments of the sodium channels shows no evident pattern for the overall effect of each phenotype based on their distributions across structural segments (Figure 8). There is even no significant preference for GoF_o (or LoF_o) phenotypes for their structural distributions. Only in the case of CMD1E ($Na_v1.5$) are all mutations located in one structural segment (VSDs). Additionally, the mutations associated with ASD and HOKPP2 are located in only two structural segments. For most other phenotypes, mutations are found in at least three distinct structural segments. This observation underlines the fact that mutations across

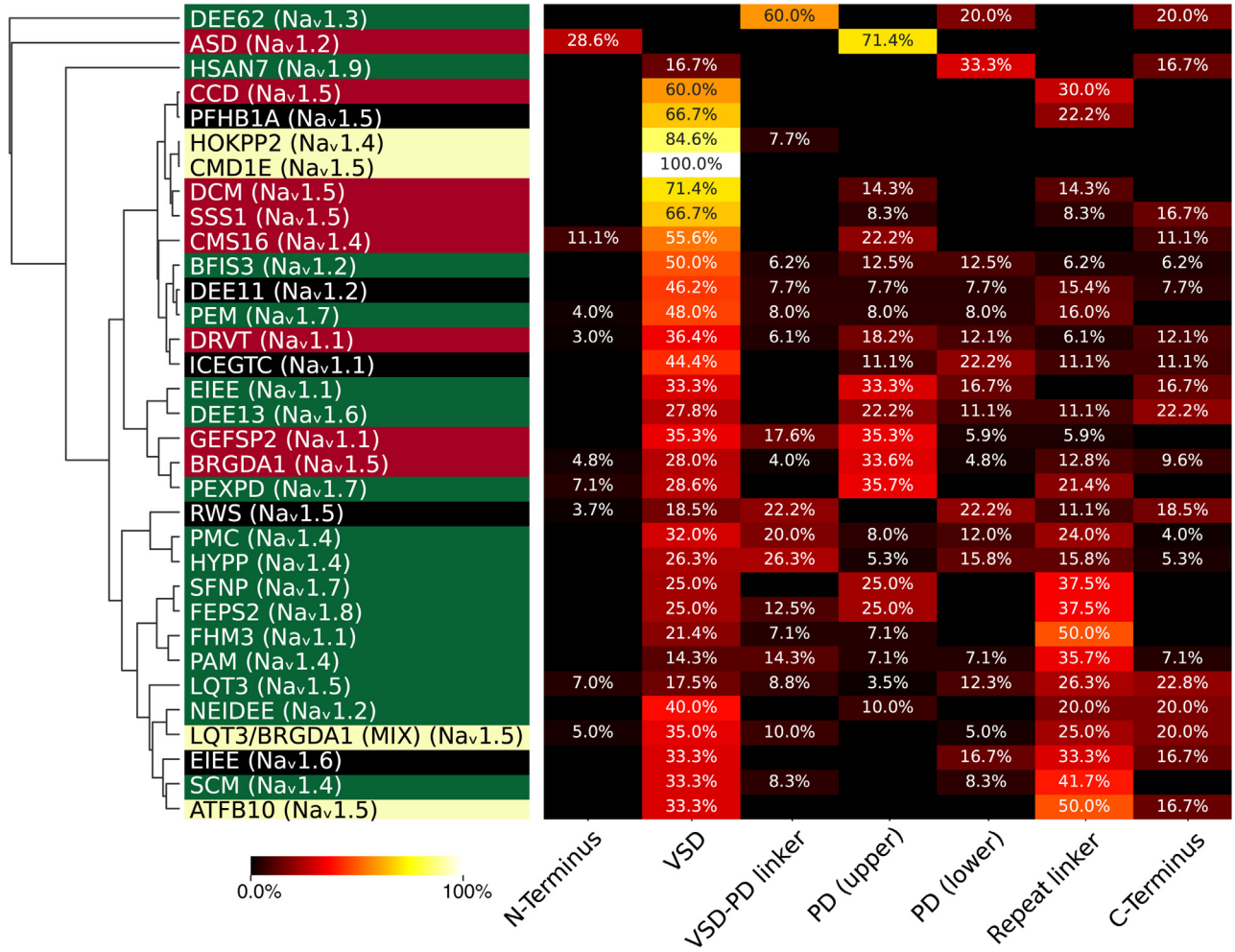

Figure 8. Mapping the phenotypes based on the gating-property impacts of associated mutations

Phenotype clustering of missense mutation in Na_v based on the similarity of gating-property impacts. Black cells represent no data for the corresponding disease segment. The heatmap is colored based on the percentage (%) of mutations affecting a certain gating property within a specific phenotype. Diseases are colored in green (GoF_o), red (LoF_o), yellow (MiX_o), and black for undetermined phenotypes. Please check the supplementary materials for a colorblind-friendly version of this figure.

different regions of the sodium channels are capable of similarly altering the channel function, leading to comparable phenotypic effects. It highlights the complexity of the relationships between genetic mutations, the structural domains of ion channels, and the phenotypic outcomes of these mutations, suggesting that the overall effect on channel function is determined by a combination of alterations in multiple channel properties and regions.

On the other hand, when a phenotype displays a dominant distribution in specific structural segments, it often aligns with the structural preference for gating properties. For instance, mutations situated in VSD-PD linkers and D linkers preferentially demonstrate a GoF_o effect. Correspondingly, conditions such as DEE62 ($Na_v1.3$), where 60% of mutations are located in the VSD-PD linker, and several other phenotypes (including FHM3($Na_v1.1$) and SCM($Na_v1.4$)) with close to 50% mutations in repeat linkers, are mainly categorized as GoF_o overall effect phenotypes (Figure 8). In contrast, a large portion of mutations in the upper pore domain (PD (upper)) reduce the maximum current (I_{max}), causing a loss of function (LoF_{GP}) effect. Several phenotypes with over 30% mutations in PD (upper), such as ASD ($Na_v1.2$), BRGDA1 ($Na_v1.5$), and GEFSP2 ($Na_v1.1$), tend to be classified as LoF_o phenotypes. Nonetheless, there are exceptions showing a GoF_o effect, including PEPD ($Na_v1.7$) and EIEE ($Na_v1.1$). There is only one phenotype, HSAN7 ($Na_v1.9$), with over 30% mutations in the lower pore domain (PD (lower)). HSAN7 ($Na_v1.9$), along with several other diseases with over 20% mutations in PD (lower) (such as DEE62($Na_v1.3$) and EIEE ($Na_v1.6$)), tend to show GoF_o overall effect phenotypes. Many phenotypes exhibit 30% mutations in VSDs, but there is no clear preference for GoF_o or LoF_o effect. This is congruent with the observation that mutations in the VSD have diverse impacts on all gating properties and display modest preferences on a range of gating properties.

Pathogenic mutations are rich in arginine

In terms of amino acid mutation frequencies, a significant feature is that the pathogenic mutations of arginines (Arg) are enriched in voltage-gated sodium channels. The probability of a disease mutation at different amino acids was calculated and shown in Figure S1A. For comparison, the probability of benign or uncertain mutations and expected frequencies were also calculated (Figure S1B). Accordingly, a mutation at an Arg residue has the highest probability of causing a disease. These results demonstrate the influence probability of the specific amino acid change across the variants. As a positively charged amino acid, Arg is often involved in many essential biochemical processes. Arg mutation is well-known for its high pathogenicity mainly due to the fact that Arg mutates to residues with very different chemical properties, such as glutamine (Gln), glycine (Gly), cysteine (Cys), histidine (His), and tryptophan (Trp).[80] Different from Arg, another positively charged residue, lysine (Lys) shows the lowest relative pathogenicity in its mutations. This difference indicates that the highest probability of disease mutations at Arg may be related to important and unique structural roles in voltage-gated ion channels.

Almost all Arg mutation hotspots are located in three critical regions. These Arg residues either work as gating charges in VSDs, located in the upper part of PD behind the SF, or distributed in intracellular loops. As the essential voltage sensors in VSDs, it is reasonable that the mutations of gating charges change activation or inactivation voltage dependence and then induce dysfunctions of ion channels. ~70% of the gating-charge mutations exhibit a strong preference to hyperpolarize $V_{1/2\ Inact}$. The Args behind the SF, such as R367, R383, R878, and R893, form salt bridges with negatively charged residues (Figure 7A). Breaking critical salt bridges, these Arg mutations can induce the conformational changes of the SF and then reduce the ion permeability. Meanwhile, pathogenic Arg mutations are also popular in different intracellular loops, such as R104 in the N-terminal, R965 in repeat (II-III) linker, R1583 in S2-3 linker of VSD4, R1644 in VSD-PD linker of repeat 4, and R1826 as well as R1898 in the C-terminal. Due to their locations, these Arg may play key roles in fast inactivation, persistent current, membrane protein orientation,[81] protein-lipid interactions,[82] protein-protein interactions,[83] and even interaction between residues and PTMs. All of these pathogenic Arg mutations indicate that Na_v channels evolved diverse voltage-dependent mechanisms, not only for activation/inactivation, but also for regulation by lipids, PTMs, or other proteins.

DISCUSSION

The ability to predict variant effects on gating properties based on their structural location is highly dependent on the precise location of the mutation. Mutations in the PD (upper), particularly those near the SF, are highly likely to significantly reduce the I_{max} (Figure 4). Conversely, within the PD (lower), mutations in the FIR are likely to shift $V_{1/2\ Inact}$ in the depolarizing direction, while mutations in the AG often enhance I_p (Figure 4). For mutations within the VSDs, predicting their impacts on gating properties proves to be a challenging task. Our analysis illustrates that mutations in VSDs can have a broad range of effects on all gating properties with modest preferences toward $V_{1/2\ Act}$, $V_{1/2\ Inact}$, τ_{rec}, and I_{max}. As the voltage-sensing components of Na_v channels, VSDs initiate all three major functional transitions: activation, inactivation, and recovery.[22,68] Mutations within VSDs can either enhance or reduce channel activity by altering the structural transition between the resting ("down") and activated/inactivated ("up") states. When a mutation introduces or disrupts specific interactions, it could potentially influence the conformational equilibrium between the "up" and "down" states, as well as the rates of their transitions. In some instances, mutations can result in leaky channels directly via the VSD, leading to the generation of omega pore currents (I_{ω}). These combined factors account for the extensive range of functional effects associated with VSD mutations, providing a structural foundation for their diverse impacts. The impacts of VSD mutations are highly sensitive to the structural context of the mutated residue. Notably, this structural context is dependent on the state, selective to the subtype, and varies across VSDs of the same channel. Therefore, theoretically, if the interactions between a specific residue and its neighboring amino acids (or other molecules) across multiple functional states (including intermediates between the "down" and "up" states) are known, it could be possible to predict its impacts on gating properties based on structures in different functional states.

Our analysis shows that the mapping of phenotypes to their mutant-located structural segments does not reveal a significant correlation between structural distribution and phenotypes. The weak relationship between phenotype and structural distribution could be attributed to several factors. First, residues in different structural segments may have similar impacts on gating properties. Consequently, mutants associated with the same phenotype are not necessarily concentrated in a specific structural segment. Second, the number of identified mutations for many phenotypes is still insufficient, and the accuracy of phenotype association requires improvement. With the discovery of more disease-associated mutations, a clearer pattern may emerge linking the structural distribution of mutations, their effects on gating properties, and associated phenotypes. Thus, the ongoing discovery and characterization of disease-associated mutations will likely continue to refine our understanding of the relationship between mutations, structural segments, gating properties, and diseases.

The study's mapping of gating-property impacts on 34 sodium channelopathies reveals that even within the same overall effect (GoF_o or LoF_o) classification, different phenotypes demonstrate unique patterns of gating property alterations. This suggests that the same overall effect (either GoF_o or LoF_o) can result from different molecular mechanisms. The similarities in overall effects across certain phenotypes may be coincidental and arise from dominant impacts of different gating properties or accumulative effects of distinctive alterations. This finding highlights the challenges of the binary prediction model of gain or loss of function, both for interpreting pathophysiology and designing personalized treatments. Conversely, phenotypes belonging to the same sub-branch (as shown in Figure 3), such as PEPD ($Na_v1.7$) vs. LQT3 ($Na_v1.5$), show high similarities in gating properties. This implies that categorizing diseases based on altered gating properties may provide a more accurate clustering of diseases driven by similar pathophysiological mechanisms. This nuanced understanding of gating property impacts has the potential to improve prediction accuracy and the design of more effective treatments. There may also be opportunities for repurposing drugs that treat a particular phenotype for the treatment of other diseases with a similar effect on gating properties.

Limitations of the study

We would like to note several potential limitations that suggest a cautious interpretation of the data collected in this study. Firstly, despite efforts to standardize, the electrophysiological experiments included in this study were conducted under varying conditions in different papers. Similarly, not all gating properties were measured uniformly across these experiments, with some, such as I_{max}, being more frequently reported than others, like I_{∞}, leading to a disproportionate representation in this dataset. In addition, terminologies such as "overall GoF" and "LoF" are not always consistently defined across different studies. The GoF/LoF at the molecular level might be mixed with effects at the cellular level and nuanced descriptions like "mild" or "moderate" GoF/LoF could be used for benign cases as well. Furthermore, there might be an ascertainment bias in the phenotypic and electrophysiological data collected, as well as potential uncertainties arising from pooling variants from different genes, which may not behave uniformly in different cell environments. It is recommended to consider all these factors when repurposing the dataset for other studies.

RESOURCE AVAILABILITY

Lead contact

Further information and requests for further information and resources should be directed to lead contact, Dr. Jing Li (jli15@olemiss.edu).

Materials availability

This study did not generate new unique reagents.

Data and code availability

- Data: This paper analyzes existing, publicly available data. The accession numbers for the datasets are listed in the key resources table. All data have been reported as supplementary material and are attached with the paper.
- Code: This paper does not report original code. The code related to the analysis can be accessed by reaching out to the lead contact.
- Additional Information: Any additional information required to reanalyze the data reported in this paper is available from the lead contact upon request.

ACKNOWLEDGMENTS

Discussions with Drs. Claudio Grosman, Joao Luis Carvalho De Souza, John Bankston, and Tamer M. Gamal El-Din are gratefully acknowledged. Computer resources came from a Maximize ACCESS allocation through project BIO210015, an allocation (MCB200085P) on Antons at the Pittsburgh Supercomputing Center provided by the National Center for Multiscale Modeling of Biological Systems through National Institutes of Health grant P41GM103712-1 and from a loan from D.E. Shaw Research, and a Frontera Pathways allocation (MCB21012) at the Texas Advanced Computing Center (TACC). Research reported in this publication was supported by an Institutional Development Award (IDeA) from the National Institute of General Medical Sciences of the National Institutes of Health under award number P20GM130460, the Data Science/AI Research Seed grant (SB3002 IDS RSG-03), and an IDS Data Science and AI Fellowship from Institute for Data Science at the University of Mississippi.

AUTHOR CONTRIBUTIONS

Conceptualization: A.A., E.E., H.B., and J.L.; methodology: J.L. and A.A.; investigation: A.A., E.E., and H.B.; visualization: A.A.; supervision: J.L.; writing—original draft: J.L.; writing—review and editing: A.A., E.E., H.B., and J.L.

DECLARATION OF INTERESTS

The authors declare no competing interests.

DECLARATION OF GENERATIVE AI AND AI-ASSISTED TECHNOLOGIES IN THE WRITING PROCESS

During the preparation of this work, the author(s) used ChatGPT in order to assist with polishing the text. After using this tool/service, the author(s) reviewed and edited the content as needed and take(s) full responsibility for the content of the publication.

STAR★METHODS

Detailed methods are provided in the online version of this paper and include the following:

SUPPLEMENTAL INFORMATION

Supplemental information can be found online at https://doi.org/10.1016/j.isci.2024.110678.

Received: January 9, 2024
Revised: June 18, 2024
Accepted: August 2, 2024
Published: August 23, 2024

REFERENCES

1. Alexander, S.P.H., Mathie, A.A., Peters, J.A., Veale, E.L., Striessnig, J., Kelly, E., Armstrong, J.F., Faccenda, E., Harding, S.D., Davies, J.A., et al. (2023). The Concise Guide to PHARMACOLOGY 2023/24: Ion channels. Br. J. Pharmacol. *180*, S145–S222. https://doi.org/10.1111/BPH.16178.
2. Mantegazza, M., Cestèle, S., and Catterall, W.A. (2021). Sodium Channelopathies of Skeletal Muscle and Brain. Physiol. Rev. *101*, 1633–1689. https://doi.org/10.1152/physrev.00025.2020.
3. Pan, X., Li, Z., Zhou, Q., Shen, H., Wu, K., Huang, X., Chen, J., Zhang, J., Zhu, X., Lei, J., et al. (2018). Structure of the human voltage-gated sodium channel Nav1.4 in complex with beta1. Science *362*, eaau2486. https://doi.org/10.1126/science.aau2486.
4. Ghovanloo, M.R., Aimar, K., Ghadiry-Tavi, R., Yu, A., and Ruben, P.C. (2016). Physiology and Pathophysiology of Sodium Channel Inactivation. Curr. Top. Membr. *78*, 479–509. https://doi.org/10.1016/bs.ctm.2016.04.001.
5. George, A.L. (2005). Inherited disorders of voltage-gated sodium channels. J. Clin. Invest. *115*, 1990–1999. https://doi.org/10.1172/JCI25505.
6. Huang, W., Liu, M., Yan, S.F., and Yan, N. (2017). Structure-based assessment of disease-related mutations in human voltage-gated sodium channels. Protein Cell *8*, 401–438. https://doi.org/10.1007/s13238-017-0372-z.
7. Mantegazza, M., Cestèle, S., and Catterall, W.A. (2021). Sodium channelopathies of skeletal muscle and brain. Physiol. Rev. *101*, 1633–1689. https://doi.org/10.1152/PHYSREV.00025.2020.
8. Liu, M., Yang, K.C., and Dudley, S.C. (2014). Cardiac Sodium Channel Mutations: Why So Many Phenotypes? Nat. Rev. Cardiol. *11*, 607–615. https://doi.org/10.1038/nrcardio.2014.85.
9. Wilde, A.A.M., and Amin, A.S. (2018). Clinical Spectrum of SCN5A Mutations: Long QT Syndrome, Brugada Syndrome, and Cardiomyopathy. JACC. Clin. Electrophysiol. *4*, 569–579. https://doi.org/10.1016/J.JACEP.2018.03.006.
10. Nicole, S., and Fontaine, B. (2015). Skeletal muscle sodium channelopathies. Curr. Opin. Neurol. *28*, 508–514. https://doi.org/10.1097/WCO.0000000000000238.
11. Meisler, M.H., Hill, S.F., and Yu, W. (2021). Sodium channelopathies in neurodevelopmental disorders. Nat. Rev. Neurosci. *22*, 152–166. https://doi.org/10.1038/s41583-020-00418-4.
12. Drenth, J.P.H., and Waxman, S.G. (2007). Mutations in sodium-channel gene SCN9A cause a spectrum of human genetic pain disorders. J. Clin. Invest. *117*, 3603–3609. https://doi.org/10.1172/JCI33297.
13. Vetter, I., Deuis, J.R., Mueller, A., Israel, M.R., Starobova, H., Zhang, A., Rash, L.D., and Mobli, M. (2017). NaV1.7 as a pain target – From gene to pharmacology. Pharmacol. Ther. *172*, 73–100. https://doi.org/10.1016/j.pharmthera.2016.11.015.
14. Catterall, W.A. (2012). Voltage-gated sodium channels at 60: structure, function and pathophysiology. J. Physiol. *590*, 2577–2589. https://doi.org/10.1113/JPHYSIOL.2011.224204.
15. Brunklaus, A., Ellis, R., Reavey, E., Semsarian, C., and Zuberi, S.M. (2014). Genotype phenotype associations across the voltage-gated sodium channel family. J. Med. Genet. *51*, 650–658. https://doi.org/10.1136/jmedgenet-2014-102608.
16. Sanders, S.J., Campbell, A.J., Cottrell, J.R., Moller, R.S., Wagner, F.F., Auldridge, A.L., Bernier, R.A., Catterall, W.A., Chung, W.K., Empfield, J.R., et al. (2018). Progress in Understanding and Treating SCN2A-Mediated Disorders. Trends Neurosci. *41*, 442–456. https://doi.org/10.1016/j.tins.2018.03.011.
17. Heyne, H.O., Baez-Nieto, D., Iqbal, S., Palmer, D.S., Brunklaus, A., May, P., Epi25 Collaborative, Johannesen, K.M., Lauxmann, S., Lemke, J.R., et al. (2020). Predicting functional effects of missense variants in voltage-gated sodium and calcium channels. Sci. Transl. Med. *12*, 6848. https://doi.org/10.1126/SCITRANSLMED.AAY6848.
18. Boßelmann, C.M., Hedrich, U.B.S., Lerche, H., and Pfeifer, N. (2023). Predicting functional effects of ion channel variants using new phenotypic machine learning methods. PLoS Comput. Biol. *19*, e1010959. https://doi.org/10.1371/JOURNAL.PCBI.1010959.
19. Brunklaus, A., Feng, T., Brünger, T., Perez-Palma, E., Heyne, H., Matthews, E., Semsarian, C., Symonds, J.D., Zuberi, S.M., Lal, D., and Schorge, S. (2022). Gene variant effects across sodium channelopathies predict function and guide precision therapy. Brain *145*, 4275–4286. https://doi.org/10.1093/BRAIN/AWAC006.
20. Holland, K.D., Bouley, T.M., and Horn, P.S. (2018). A surrogate for personalized treatment of sodium channelopathies. Ann. Neurol. *84*, 1–9. https://doi.org/10.1002/ANA.25268.
21. Koch, N.A., Sonnenberg, L., Hedrich, U.B.S., Lauxmann, S., and Benda, J. (2023). Loss or gain of function? Effects of ion channel mutations on neuronal firing depend on the neuron type. Front. Neurol. *14*, 1194811. https://doi.org/10.3389/FNEUR.2023.1194811/BIBTEX.
22. Catterall, W.A., Wisedchaisri, G., and Zheng, N. (2020). The conformational cycle of a prototypical voltage-gated sodium channel. Nat. Chem. Biol. *16*, 1314–1320. https://doi.org/10.1038/s41589-020-0644-4.
23. Ruan, Y., Liu, N., and Priori, S.G. (2009). Sodium channel mutations and arrhythmias. Nat. Rev. Cardiol. *6*, 337–348. https://doi.org/10.1038/nrcardio.2009.44.
24. Li, W., Yin, L., Shen, C., Hu, K., Ge, J., and Sun, A. (2018). SCN5A variants: Association with cardiac disorders. Front. Physiol. *9*, 1372–1413. https://doi.org/10.3389/fphys.2018.01372.
25. Remme, C.A., Wilde, A.A.M., and Bezzina, C.R. (2008). Cardiac Sodium Channel Overlap Syndromes: Different Faces of SCN5A Mutations. Trends Cardiovasc. Med. *18*, 78–87. https://doi.org/10.1016/j.tcm.2008.01.002.
26. Li, Z., Jin, X., Wu, T., Zhao, X., Wang, W., Lei, J., Pan, X., and Yan, N. (2021). Structure of human Nav1.5 reveals the fast inactivation-related segments as a mutational hotspot for the long QT syndrome. Proc. Natl. Acad. Sci. USA *118*, e2100069118. https://doi.org/10.1073/PNAS.2100069118.
27. Millat, G., Chevalier, P., Restier-Miron, L., da Costa, A., Bouvagnet, P., Kugener, B., Fayol, L., Gonzàlez Armengod, C., Oddou, B., Chanavat, V., et al. (2006). Spectrum of pathogenic mutations and associated polymorphisms in a cohort of 44 unrelated patients with long QT syndrome. Clin. Genet. *70*, 214–227. https://doi.org/10.1111/j.1399-0004.2006.00671.x.
28. Kapplinger, J.D., Tester, D.J., Alders, M., Benito, B., Berthet, M., Brugada, J., Brugada, P., Fressart, V., Guerchicoff, A., Harris-Kerr, C., et al. (2010). An international compendium of mutations in the SCN5A-encoded cardiac sodium channel in patients referred for Brugada syndrome genetic testing. Heart Rhythm *7*, 33–46. https://doi.org/10.1016/j.hrthm.2009.09.069.
29. Li, G., Woltz, R.L., Wang, C.Y., Ren, L., He, P.X., Yu, S.D., Liu, X.Q., Yarov-Yarovoy, V., Hu, D., Chiamvimonvat, N., and Wu, L. (2020). Gating Properties of Mutant Sodium Channels and Responses to Sodium Current Inhibitors Predict Mexiletine-Sensitive Mutations of Long QT Syndrome 3. Front. Pharmacol. *11*, 1182. https://doi.org/10.3389/fphar.2020.01182.
30. Glazer, A.M., Wada, Y., Li, B., Muhammad, A., Kalash, O.R., O'Neill, M.J., Shields, T., Hall, L., Short, L., Blair, M.A., et al. (2020). High-Throughput Reclassification of SCN5A Variants. Am. J. Hum. Genet. *107*, 111–123. https://doi.org/10.1016/j.ajhg.2020.05.015.
31. Holland, K.D., Kearney, J.A., Glauser, T.A., Buck, G., Keddache, M., Blankston, J.R., Glaaser, I.W., Kass, R.S., and Meisler, M.H. (2008). Mutation of sodium channel SCN3A in a patient with cryptogenic pediatric partial epilepsy. Neurosci. Lett. *433*, 65–70. https://doi.org/10.1016/J.NEULET.2007.12.064.
32. Wu, M.T., Huang, P.Y., Yen, C.T., Chen, C.C., and Lee, M.J. (2013). A Novel SCN9A Mutation Responsible for Primary Erythromelalgia and Is Resistant to the Treatment of Sodium Channel Blockers. PLoS One *8*, e55212. https://doi.org/10.1371/JOURNAL.PONE.0055212.
33. Suetterlin, K.J., Bugiardini, E., Kaski, J.P., Morrow, J.M., Matthews, E., Hanna, M.G., and Fialho, D. (2015). Long-term Safety and Efficacy of Mexiletine for Patients With Skeletal Muscle Channelopathies. JAMA Neurol. *72*, 1531–1533. https://doi.org/10.1001/JAMANEUROL.2015.2338.
34. De Bellis, M., Boccanegra, B., Cerchiara, A.G., Imbrici, P., and De Luca, A. (2023). Blockers of Skeletal Muscle Nav1.4 Channels: From Therapy of Myotonic Syndrome to Molecular

Determinants of Pharmacological Action and Back. Int. J. Mol. Sci. *24*, 857. https://doi.org/10.3390/IJMS24010857.

35. Ademuwagun, I.A., Rotimi, S.O., Syrbe, S., Ajamma, Y.U., and Adebiyi, E. (2021). Voltage Gated Sodium Channel Genes in Epilepsy: Mutations, Functional Studies, and Treatment Dimensions. Front. Neurol. *12*, 600050. https://doi.org/10.3389/fneur.2021.600050.
36. Traub, R.D., Wong, R.K., Miles, R., and Michelson, H. (1991). A model of a CA3 hippocampal pyramidal neuron incorporating voltage-clamp data on intrinsic conductances. J. Neurophysiol. *66*, 635–650. https://doi.org/10.1152/JN.1991.66.2.635.
37. Chung, K.M., Hack, J., Andrews, J., Galindo-Kelly, M., Schreiber, J., Watkins, J., and Hammer, M.F. (2023). Clinical severity is correlated with age at seizure onset and biophysical properties of recurrent gain of function variants associated with SCN8A-related epilepsy. Epilepsia *64*, 3365–3376. https://doi.org/10.1111/EPI.17747.
38. Johannesen, K.M., Liu, Y., Koko, M., Gjerulfsen, C.E., Sonnenberg, L., Schubert, J., Fenger, C.D., Eltokhi, A., Rannap, M., Koch, N.A., et al. (2022). Genotype-phenotype correlations in SCN8A-related disorders reveal prognostic and therapeutic implications. Brain *145*, 2991–3009. https://doi.org/10.1093/BRAIN/AWAB321.
39. Seiffert, S., Pendziwiat, M., Bierhals, T., Goel, H., Schwarz, N., van der Ven, A., Boßelmann, C.M., Lemke, J., Syrbe, S., Willemsen, M.H., et al. (2022). Modulating effects of FGF12 variants on NaV1.2 and NaV1.6 being associated with developmental and epileptic encephalopathy and Autism spectrum disorder: A case series. EBioMedicine *83*, 104234. https://doi.org/10.1016/J.EBIOM.2022.104234.
40. Gauthier, N.P., Reznik, E., Gao, J., Sumer, S.O., Schultz, N., Sander, C., and Miller, M.L. (2016). MutationAligner: A resource of recurrent mutation hotspots in protein domains in cancer. Nucleic Acids Res. *44*, D986–D991. https://doi.org/10.1093/nar/gkv1132.
41. Miller, M.L., Reznik, E., Gauthier, N.P., Aksoy, B.A., Korkut, A., Gao, J., Ciriello, G., Schultz, N., and Sander, C. (2015). Pan-Cancer Analysis of Mutation Hotspots in Protein Domains. Cell Syst. *1*, 197–209. https://doi.org/10.1016/J.CELS.2015.08.014.
42. Noreng, S., Li, T., and Payandeh, J. (2021). Structural Pharmacology of Voltage-Gated Sodium Channels. J. Mol. Biol. *433*, 166967. https://doi.org/10.1016/J.JMB.2021.166967.
43. Famiglietti, M.L., Estreicher, A., Gos, A., Bolleman, J., Géhant, S., Breuza, L., Bridge, A., Poux, S., Redaschi, N., Bougueleret, L., et al. (2014). Genetic variations and diseases in UniProtKB/Swiss-Prot: The ins and outs of expert manual curation. Hum. Mutat. *35*, 927–935. https://doi.org/10.1002/humu.22594.
44. Moreau, A., Gosselin-Badaroudine, P., and Chahine, M. (2014). Biophysics, Pathophysiology, and Pharmacology of Ion Channel Gating Pores. Front. Pharmacol. *5*, 53. https://doi.org/10.3389/fphar.2014.00053.
45. Jurkat-Rott, K., Groome, J., and Lehmann-Horn, F. (2012). Pathophysiological role of omega pore current in channelopathies. Front. Pharmacol. *3*, 112. https://doi.org/10.3389/fphar.2012.00112.
46. Sokolov, S., Scheuer, T., and Catterall, W.A. (2007). Gating pore current in an inherited ion channelopathy. Nature *446*, 76–78. https://doi.org/10.1038/nature05598.
47. Struyk, A.F., Markin, V.S., Francis, D., and Cannon, S.C. (2008). Gating pore currents in DIIS4 mutations of NaV1.4 associated with periodic paralysis: Saturation of ion flux and implications for disease pathogenesis. J. Gen. Physiol. *132*, 447–464. https://doi.org/10.1085/jgp.200809967.
48. Moreau, A., Gosselin-Badaroudine, P., Delemotte, L., Klein, M.L., and Chahine, M. (2015). Gating pore currents are defects in common with two Nav1.5 mutations in patients with mixed arrhythmias and dilated cardiomyopathy. J. Gen. Physiol. *145*, 93–106. https://doi.org/10.1085/JGP.201411304.
49. Starace, D.M., and Bezanilla, F. (2004). A proton pore in a potassium channel voltage sensor reveals a focused electric field. Nature *1*, 548–553. https://doi.org/10.1038/nature02270.
50. Kapplinger, J.D., Tester, D.J., Salisbury, B.A., Carr, J.L., Harris-Kerr, C., Pollevick, G.D., Wilde, A.A., and Ackerman, M.J. (2009). Spectrum and prevalence of mutations from the first 2,500 consecutive unrelated patients referred for the FAMILION long QT syndrome genetic test. Heart Rhythm *6*, 1297–1303. https://doi.org/10.1016/J.HRTHM.2009.05.021.
51. Makita, N., Shirai, N., Nagashima, M., Matsuoka, R., Yamada, Y., Tohse, N., and Kitabatake, A. (1998). A de novo missense mutation of human cardiac Na+ channel exhibiting novel molecular mechanisms of long QT syndrome. FEBS Lett. *423*, 5–9. https://doi.org/10.1016/S0014-5793(98)00033-7.
52. Lee, S.-C., Kim, H.-S., Park, Y.-E., Choi, Y.-C., Park, K.-H., and Kim, D.-S. (2009). Clinical Diversity of SCN4A-Mutation-Associated Skeletal Muscle Sodium Channelopathy. J. Clin. Neurol. *5*, 186–191. https://doi.org/10.3988/JCN.2009.5.4.186.
53. Zaharieva, I.T., Thor, M.G., Oates, E.C., van Karnebeek, C., Hendson, G., Blom, E., Witting, N., Rasmussen, M., Gabbett, M.T., Ravenscroft, G., et al. (2016). Loss-of-function mutations in SCN4A cause severe foetal hypokinesia or 'classical' congenital myopathy. Brain *139*, 674–691. https://doi.org/10.1093/BRAIN/AWV352.
54. Clairfeuille, T., Xu, H., Koth, C.M., and Payandeh, J. (2017). Voltage-gated sodium channels viewed through a structural biology lens. Curr. Opin. Struct. Biol. *45*, 74–84. https://doi.org/10.1016/j.sbi.2016.11.022.
55. Wisedchaisri, G., Tonggu, L., Gamal El-Din, T.M., McCord, E., Zheng, N., and Catterall, W.A. (2021). Structural Basis for High-Affinity Trapping of the NaV1.7 Channel in Its Resting State by Tarantula Toxin. Mol. Cell *81*, 38–48.e4. https://doi.org/10.1016/J.MOLCEL.2020.10.039.
56. Huang, G., Wu, Q., Li, Z., Jin, X., Huang, X., Wu, T., Pan, X., and Yan, N. (2022). Unwinding and spiral sliding of S4 and domain rotation of VSD during the electromechanical coupling in Nav1.7. Proc. Natl. Acad. Sci. USA *119*, e2209164119. https://doi.org/10.1073/PNAS.2209164119.
57. Groome, J.R., and Bayless-Edwards, L. (2020). Roles for Countercharge in the Voltage Sensor Domain of Ion Channels. Front Pharmacol. *11*, 160. https://doi.org/10.3389/fphar.2020.00160.
58. Jurkat-Rott, K., Groome, J., and Lehmann-Horn, F. (2012). Pathophysiological role of omega pore current in channelopathies. Front. Pharmacol. *3*, 112. https://doi.org/10.3389/FPHAR.2012.00112.
59. Liu, Y., Koko, M., and Lerche, H. (2021). A SCN8A variant associated with severe early onset epilepsy and developmental delay: Loss- or gain-of-function? Epilepsy Res. *178*, 106824. https://doi.org/10.1016/J.EPLEPSYRES.2021.106824.
60. Mason, E.R., Wu, F., Patel, R.R., Xiao, Y., Cannon, S.C., and Cummins, T.R. (2019). Resurgent and Gating Pore Currents Induced by De Novo SCN2A Epilepsy Mutations. eNeuro *6*, 1. https://doi.org/10.1523/ENEURO.0141-19.2019.
61. Kuzmenkin, A., Muncan, V., Jurkat-Rott, K., Hang, C., Lerche, H., Lehmann-Horn, F., and Mitrovic, N. (2002). Enhanced inactivation and pH sensitivity of Na+ channel mutations causing hypokalaemic periodic paralysis type II. Brain *125*, 835–843. https://doi.org/10.1093/BRAIN/AWF071.
62. Jurkat-Rott, K., Mitrovic, N., Hang, C., Kouzmekine, A., Iaizzo, P., Herzog, J., Lerche, H., Nicole, S., Vale-Santos, J., Chauveau, D., et al. (2000). Voltage-sensor sodium channel mutations cause hypokalemic periodic paralysis type 2 by enhanced inactivation and reduced current. Proc. Natl. Acad. Sci. USA *97*, 9549–9554. https://doi.org/10.1073/PNAS.97.17.9549.
63. Nair, K., Pekhletski, R., Harris, L., Care, M., Morel, C., Farid, T., Backx, P.H., Szabo, E., and Nanthakumar, K. (2012). Escape capture bigeminy: Phenotypic marker of cardiac sodium channel voltage sensor mutation R222Q. Heart Rhythm *9*, 1681–1688.e1. https://doi.org/10.1016/J.HRTHM.2012.06.029.
64. Mann, S.A., Castro, M.L., Ohanian, M., Guo, G., Zodgekar, P., Sheu, A., Stockhammer, K., Thompson, T., Playford, D., Subbiah, R., et al. (2012). R222Q SCN5A Mutation Is Associated With Reversible Ventricular Ectopy and Dilated Cardiomyopathy. J. Am. Coll. Cardiol. *60*, 1566–1573. https://doi.org/10.1016/J.JACC.2012.05.050.
65. Daniel, L.L., Yang, T., Kroncke, B., Hall, L., Stroud, D., and Roden, D.M. (2019). SCN5A variant R222Q generated abnormal changes in cardiac sodium current and action potentials in murine myocytes and Purkinje cells. Heart Rhythm *16*, 1676–1685. https://doi.org/10.1016/J.HRTHM.2019.05.017.
66. Gosselin-Badaroudine, P., Delemotte, L., Moreau, A., Klein, M.L., and Chahine, M. (2012). Gating pore currents and the resting state of Nav1.4 voltage sensor domains. Proc. Natl. Acad. Sci. USA *109*, 19250–19255. https://doi.org/10.1073/PNAS.1217990109.
67. Chanda, B., and Bezanilla, F. (2002). Tracking voltage-dependent conformational changes in skeletal muscle sodium channel during activation. J. Gen. Physiol. *120*, 629–645. https://doi.org/10.1085/jgp.20028679.
68. Goldschen-Ohm, M.P., Capes, D.L., Oelstrom, K.M., and Chanda, B. (2013). Multiple pore conformations driven by asynchronous movements of voltage sensors in a eukaryotic sodium channel. Nat. Commun. *4*, 1350. https://doi.org/10.1038/ncomms2356.
69. Capes, D.L., Goldschen-Ohm, M.P., Arcisio-Miranda, M., Bezanilla, F., and Chanda, B. (2013). Domain IV voltage-sensor movement is both sufficient and rate limiting for fast inactivation in sodium channels. J. Gen.

Physiol. *142*, 101–112. https://doi.org/10.1085/JGP.201310998.

70. Zhang, Y., Wang, T., Ma, A., Zhou, X., Gui, J., Wan, H., Shi, R., Huang, C., Grace, A.A., Huang, C.H., and Trump, D. (2008). Correlations between clinical and physiological consequences of the novel mutation R878C in a highly conserved pore residue in the cardiac Na+ channel. Acta Physiol. *194*, 311–323. https://doi.org/10.1111/J.1748-1716.2008.01883.X.
71. Smits, J.P.P., Eckardt, L., Probst, V., Bezzina, C.R., Schott, J.J., Remme, C.A., Haverkamp, W., Breithardt, G., Escande, D., Schulze-Bahr, E., et al. (2002). Genotype-phenotype relationship in Brugada syndrome: electrocardiographic features differentiate SCN5A-related patients from non–SCN5A-related patients. J. Am. Coll. Cardiol. *40*, 350–356. https://doi.org/10.1016/S0735-1097(02)01962-9.
72. Meregalli, P.G., Tan, H.L., Probst, V., Koopmann, T.T., Tanck, M.W., Bhuiyan, Z.A., Sacher, F., Kyndt, F., Schott, J.J., Albuisson, J., et al. (2009). Type of SCN5A mutation determines clinical severity and degree of conduction slowing in loss-of-function sodium channelopathies. Heart Rhythm *6*, 341–348. https://doi.org/10.1016/J.HRTHM.2008.11.009.
73. Cowgill, J., and Chanda, B. (2021). Mapping Electromechanical Coupling Pathways in Voltage-Gated Ion Channels: Challenges and the Way Forward. J. Mol. Biol. *433*, 167104. https://doi.org/10.1016/J.JMB.2021.167104.
74. Shen, H., Zhou, Q., Pan, X., Li, Z., Wu, J., and Yan, N. (2017). Structure of a eukaryotic voltage-gated sodium channel at near-atomic resolution. Science *355*, eaal4326. https://doi.org/10.1126/science.aal4326.
75. Tester, D.J., Will, M.L., Haglund, C.M., and Ackerman, M.J. (2005). Compendium of cardiac channel mutations in 541 consecutive unrelated patients referred for long QT syndrome genetic testing. Heart Rhythm *2*, 507–517. https://doi.org/10.1016/J.HRTHM.2005.01.020.
76. Catterall, W.A. (2000). From Ionic Currents to Molecular Mechanisms: The Structure and Function of Voltage-Gated Sodium Channels. Neuron *26*, 13–25. https://doi.org/10.1016/S0896-6273(00)81133-2.
77. West, J.W., Patton, D.E., Scheuer, T., Wang, Y., Goldin, A.L., and Catterall, W.A. (1992). A cluster of Hydrophobic amino acid residues required for fast Na+-channel inactivation. Proc. Natl. Acad. Sci. USA *89*, 10910–10914. https://doi.org/10.1073/PNAS.89.22.10910.
78. Yan, Z., Zhou, Q., Wang, L., Wu, J., Zhao, Y., Huang, G., Peng, W., Shen, H., Lei, J., and Yan, N. (2017). Structure of the Nav1.4-β1 Complex from Electric Eel. Cell *170*, 470–482.e11. https://doi.org/10.1016/j.cell.2017.06.039.
79. Pan, X., Li, Z., Zhou, Q., Shen, H., Wu, K., Huang, X., Chen, J., Zhang, J., Zhu, X., Lei, J., et al. (2018). Structure of the human voltage-gated sodium channel Nav1.4 in complex with β1. Science *362*, eaau2486. https://doi.org/10.1126/SCIENCE.AAU2486.
80. Vitkup, D., Sander, C., and Church, G.M. (2003). The amino-acid mutational spectrum of human genetic disease. Genome Biol. *4*, R72. https://doi.org/10.1186/GB-2003-4-11-R72.
81. Nilsson, J., Persson, B., and von Heijne, G. (2005). Comparative analysis of amino acid distributions in integral membrane proteins from 107 genomes. Proteins *60*, 606–616. https://doi.org/10.1002/PROT.20583.
82. Schmidt, D., Jiang, Q.-X., and MacKinnon, R. (2006). Phospholipids and the origin of cationic gating charges in voltage sensors. Nature *444*, 775–779. https://doi.org/10.1038/nature05416.
83. Shao, D., Okuse, K., and Djamgoz, M.B.A. (2009). Protein–protein interactions involving voltage-gated sodium channels: Post-translational regulation, intracellular trafficking and functional expression. Int. J. Biochem. Cell Biol. *41*, 1471–1481. https://doi.org/10.1016/J.BIOCEL.2009.01.016.
84. Page, M.J., Moher, D., Bossuyt, P.M., Boutron, I., Hoffmann, T.C., Mulrow, C.D., Shamseer, L., Tetzlaff, J.M., Akl, E.A., Brennan, S.E., et al. (2021). PRISMA 2020 explanation and elaboration: updated guidance and exemplars for reporting systematic reviews. BMJ *372*, n160. https://doi.org/10.1136/BMJ.N160.
85. McGarvey, P.B., Nightingale, A., Luo, J., Huang, H., Martin, M.J., and Wu, C.; UniProt Consortium (2019). UniProt genomic mapping for deciphering functional effects of missense variants. Hum. Mutat. *40*, 694–705. https://doi.org/10.1002/HUMU.23738.
86. Rozewicki, J., Li, S., Amada, K.M., Standley, D.M., and Katoh, K. (2019). MAFFT-DASH: integrated protein sequence and structural alignment. Nucleic Acids Res. *47*, W5–W10. https://doi.org/10.1093/NAR/GKZ342.
87. Troshin, P.V., Procter, J.B., and Barton, G.J. (2011). Java bioinformatics analysis web services for multiple sequence alignment–JABAWS:MSA. Bioinformatics *27*, 2001–2002. https://doi.org/10.1093/BIOINFORMATICS/BTR304.
88. Humphrey, W., Dalke, A., and Schulten, K. (1996). VMD: Visual molecular dynamics. J. Mol. Graph. *14*, 33–38. https://doi.org/10.1016/0263-7855(96)00018-5.
89. Van Rossum, G., and Drake, F.L. (2009). Python 3 Reference Manual; CreateSpace. Scotts Valley, CA, 242.
90. The pandas development team (2020). Pandas-Dev/Pandas: Pandas (Zenodo). https://doi.org/10.5281/ZENODO.7979740.
91. Harris, C.R., Millman, K.J., van der Walt, S.J., Gommers, R., Virtanen, P., Cournapeau, D., Wieser, E., Taylor, J., Berg, S., Smith, N.J., et al. (2020). Array programming with NumPy. Nature *585*, 357. https://doi.org/10.1038/s41586-020-2649-2.
92. Cock, P.J.A., Antao, T., Chang, J.T., Chapman, B.A., Cox, C.J., Dalke, A., Friedberg, I., Hamelryck, T., Kauff, F., Wilczynski, B., and de Hoon, M.J.L. (2009). Biopython: freely available Python tools for computational molecular biology and bioinformatics. Bioinformatics *25*, 1422–1423. https://doi.org/10.1093/BIOINFORMATICS/BTP163.
93. Hunter, J.D. (2007). Matplotlib: A 2D graphics environment. Comput. Sci. Eng. *9*, 90–95. https://doi.org/10.1109/MCSE.2007.55.
94. Jiang, D., Banh, R., El-Din, T.M.G., Tonggu, L., Lenaeus, M.J., Pomès, R., Zheng, N., and Catterall, W.A. (2021). Open-state structure and pore gating mechanism of the cardiac sodium channel. Cell *184*, 5151–5162.e11. https://doi.org/10.1016/J.CELL.2021.08.021.
95. Lomize, M.A., Pogozheva, I.D., Joo, H., Mosberg, H.I., and Lomize, A.L. (2012). OPM database and PPM web server: resources for positioning of proteins in membranes. Nucleic Acids Res. *40*, D370–D376. https://doi.org/10.1093/NAR/GKR703.
96. Virtanen, P., Gommers, R., Oliphant, T.E., Haberland, M., Reddy, T., Cournapeau, D., Burovski, E., Peterson, P., Weckesser, W., Bright, J., et al. (2020). SciPy 1.0: fundamental algorithms for scientific computing in Python. Nat. Methods *17*, 261. https://doi.org/10.1038/s41592-019-0686-2.
97. Bray, J.R., and Curtis, J.T. (1957). An Ordination of the Upland Forest Communities of Southern Wisconsin. Ecol. Monogr. *27*, 325–349. https://doi.org/10.2307/1942268.
98. Waterhouse, A.M., Procter, J.B., Martin, D.M.A., Clamp, M., and Barton, G.J. (2009). Jalview Version 2—a multiple sequence alignment editor and analysis workbench. Bioinformatics *25*, 1189–1191. https://doi.org/10.1093/BIOINFORMATICS/BTP033.

STAR★METHODS

KEY RESOURCES TABLE

REAGENT or RESOURCE	SOURCE	IDENTIFIER
Deposited data		
Index of Protein Altering Variants	Uniprot	2022_03
Index of human variants curated from literature reports	Uniprot	2022_03
'TITLE-ABS-KEY (SCNXA AND electrophysiology AND mutation) AND (LIMIT-TO (DOCTYPE, "ar"))	Scopus	March 29th, 2023
7DTC	https://opm.phar.umich.edu/	–
OMIM	https://www.omim.org/statistics/update	2022_AUG
Software and algorithms		
MAFFT	Jalview	5
Jalview	Jalview	2.11.2.6
VMD - Visual Molecular Dynamics	https://www.ks.uiuc.edu/Research/vmd/	1.9.4
Python	Python	3.10
Pandas	https://pandas.pydata.org/	2.0.3
Numpy	https://numpy.org/	1.25.2
BioPython	https://biopython.org/	1.81
Matplotlib	https://matplotlib.org/	3.5.2
seaborn	https://seaborn.pydata.org/	v0.12.2

METHOD DETAILS

Data gathering and search strategy

In this study, we utilized two major databases to obtain pathogenic mutations in Na_v channels and gather functional data related to these mutations.

Firstly, adhering to the PRISMA guidelines,[84] we systematically searched Scopus on March 29th, 2023, to identify English-language studies describing the functional characteristics of missense variants using the following mesh query: 'TITLE-ABS-KEY (SCNXA AND electrophysiology AND mutation) AND (LIMIT-TO (DOCTYPE, "ar")),' where X represents the corresponding sodium channel number and "ar" stands for a research article. Furthermore, we conducted a manual search of sodium channel mutation databases and reviewed relevant bibliographies obtained for our search. We specifically selected missense variants whose effects were characterized through whole-cell patch clamp electrophysiology using human Na_v channels. Mutations without any functional effects (no changes in biophysical properties) and double mutations were excluded. In cases where contradictory findings existed, duplicated data were considered as additional data points (Table S3). This process led to the selection of unique 525 mutations with their functional data (Figure 2A). Eighty mutations from this dataset were later added to the next dataset to address some missing phenotypes in UniProt (e.g., Autism Spectrum Disorder (ASD) in $Na_v1.2$). Three researchers, namely A.A.A., E.E., and H.B., independently reviewed the data.

Secondly, we utilized UniProt's "Index of Protein Altering Variants" (Release: 2022_03) in conjunction with UniProt's "Index of human variants curated from literature reports" (Release: 2022_03)[85] to extract pathogenic mutations within this protein family. We queried the combined database to identify non-cancerous missense mutations with clear OMIM disease assignments across all nine members of Na_v channels, including their respective naturally occurring isoforms (Figure 2B). Duplicate mutations resulting in the same phenotype within each family member were excluded. Manual annotations were performed to ensure consistency with OMIM, addressing certain phenotype assignments (e.g., LQTs in $Na_v1.5$ to LQT3, PEXPD to PEPD in $Na_v1.7$). This process led to the selection of 2409 mutations out of the 36.63 million presented in UniProt. Additionally, we employed a similar workflow to collect benign and uncertain mutations, resulting in a total of 10,348 mutations in this category.

Data analysis

MSA was conducted using MAFFT[86] to align all naturally occurring Na_v isoforms and was visualized in JalView[87] 2.11.2.6. Subsequently, the pathogenic mutations obtained from UniProt were mapped onto this alignment to identify recurrent mutations and their respective phenotype in each residue throughout the alignment. The number of mutations, phenotypes, and proteins associated with these variants were tallied and graphed in relation to the MSA. The top 2% of mutations meeting any of the following criteria: more than 6 phenotypes, 5 mutations,

or 4 proteins reported from a single residue position were selected as hotspots. Mapping these hotspots in protein sequences and visualizing them in 3D structure was carried out using VMD[88] and Python 3.10,[89] utilizing Pandas,[90] Numpy,[91] BioPython,[92] and Matplotlib[93] packages.

Mutations are mapped on different regions to characterize their structural distribution. The selectivity filter region (SF) is defined as including residues within 5 Å of the four filter-forming residues (D372, E898, K1419, A1711[26]). Similarly, the activation gate region (AG) also includes residues within 5 Å of gating residues (A413, L938, I1470, I1771[94]). Fast inactivation region (FIR) is the residues within 5 Å of residues (1467–1500[94]). The choice of 5 Å corresponds to a conservative range for the effective distance of non-covalent interactions, such as hydrogen bonds, hydrophobic interactions, and salt bridges, typically observed in protein structures. This distance was chosen to ensure that direct interactions are captured, but it does not preclude the possibility of longer-range effects, such as allosteric communications. The midpoints are used to separate the "upper" and "lower" portions of both PD and VSD. The midpoint is determined by calculating the z-coordinate midpoint of the lowest atom in the SF and the highest atom in the AG, whereas the midpoint of VSDs is the z-coordinate of the Cα atom of the aromatic residue (either Y or F) in the hydrophobic constriction site in each VSD. The residues in each structural selection were determined using VMD based on a $Na_v1.5$ (PDB: 7DTC[26]) structure from the Orientations of Proteins in Membranes (OPM) database.[95] All residues from other Na_v channels are also selected for each protein based on the multiple sequence alignment.

Gating properties altered by variants are documented in the literature, and they were categorized as either gain-of-function on a certain gating property (GoF_{GP}) or loss-of-function (LoF_{GP}) (Figure 1A). GoF_{GP} effects include an increase in maximal current amplitude (I_{max}), an elevation in persistent current (I_P), a decrease in the numerical values of recovery rate (τ_{rec}) from fast inactivation, a hyperpolarizing shift in half-activation voltage in steady-state activation ($V_{1/2\ Act}$), a depolarizing shift in half-inactivation voltage ($V_{1/2\ Inact}$), and the presence of inward gating pore current (or ω current, I_ω). Conversely, LoF_{GP} effects represented opposing effects on the same parameters (Figure 1A). Information regarding the phenotypes and the corresponding GoF_{GP} or LoF_{GP} assignment of each mutation, if provided in the literature, was recorded (Figure 2A). These mutations were then mapped onto distinct structural segments of the protein to examine the structural distribution of biophysical property changes (Figure 3). To assess the impact preference of a selected group of mutations (e.g., within a specific structural segment or associated with a certain disease) on a certain gating property, we calculate the GoF_{GP}/LoF_{GP} Preference Index (GLPI). The GLPI for a certain gating property *i* is determined by two factors. The first factor is calculated based on the difference between the number of relevant mutations with GoF_{GP} effect (n_{GoF}) and those with LoF_{GP} effect (n_{LoF}), divided by the total number of mutations within the selected group that affect this gating property *i*. The second factor is the percentage of the mutations impacting gating property *i* within the selected group (p_i), marked as X% in each grid of Figures 3, 4, and 8, was calculated by dividing the number of mutations showing property alterations by the total number of mutations reported for the selected group.

$$\text{GoF} \Big/ \text{LoF preference index } (GLPI_i) = \frac{n_{GoF} - n_{LoF}}{n_{GoF} + n_{LoF}} . p_i$$

The assignment of phenotypes to specific mutations required meticulous attention and involved cross-referencing various sources such as review articles, research papers, and online databases, including UniProt and OMIM. However, this task presented considerable challenges due to the limitations of manual annotation and lack of widely used standardized disease nomenclature within the field. In this study, UniProt served as the primary source for obtaining phenotype names. In instances where UniProt did not furnish a specific phenotype name, we turned to the original paper that initially reported the mutation. This approach ensured consistency in nomenclature throughout our analysis. The phenotype association dataset for mutations was subsequently clustered into different groups. This process involved iterating through various clustering algorithms and distance metrics for hyperparameter tuning using Seaborn's clustermap and employing the cosine[96,97] metric to compute the similarity:

$$d(u, v) = 1 - \frac{u.v}{||u||_2 ||v||_2}$$

where *u or v* respectively represents the GoF_{GP}/LoF_{GP} Preference Index (GLPI) of a certain group of mutations, $\| * \|_2$ is the 2-norm of its argument *, and *u.v* is the dot product of *u* and *v*. The similarity measure, $d(u, v)$, was used to assess the relative "closeness" of phenotypes based on the resulting biophysical changes (GLPI), with the average of the cosine similarities across all phenotype pairs being used to determine overall cluster cohesion.

QUANTIFICATION AND STATISTICAL ANALYSIS

Statistical analyses and software

- Software Used: MAFFT[86] for Multiple Sequence Alignment (v7.487), JalView[98] for visualization (v2.11.2.6), VMD[88] (v1.9.3), and Python[89] (v3.10) with Pandas,[90] Numpy,[91] BioPython,[92] and Matplotlib.[93].
- Statistical Tests: GoF/LoF Preference Index (GLPI) calculated to assess the impact of mutations on gating properties.

Statistical details

- n Values:
  525 unique mutations with functional data.
  2409 pathogenic mutations extracted from UniProt.

13282 total mutations including benign and uncertain variants.

- Definitions:
  GoF/LoF effects classified based on changes in gating properties.
  Hotspots identified based on thresholds: >6 phenotypes, 5 mutations, or 4 proteins per residue.
- Dispersion Measures: GLPI calculated as:

$$\text{GoF} \Big/ \text{LoF } \textit{preference index } (GLPI_i) = \frac{n_{GoF} - n_{LoF}}{n_{GoF} + n_{LoF}} . p_i$$

where n_{GoF} and n_{LoF} are the counts of GoF and LoF mutations, and p_i is the percentage of mutations affecting the property.

Significance definition

- **Significance Measures:** Differences in the GLPI values across various structural segments and phenotype groups.
- **Randomization and Sample Size**: Not applicable due to the nature of data extraction from literature and databases.
- **Inclusion/Exclusion Criteria:**
  Included: Missense variants characterized through whole-cell patch clamp electrophysiology.
  Excluded: Mutations without functional effects, double mutations, and duplicates unless showing contradictory findings.

Clustering and similarity measures

- Clustering: Seaborn's clustermap with cosine similarity used to group phenotype associations based on GLPI values.
- Cosine Similarity:

$$d(u, v) = 1 - \frac{u.v}{||u||_2 ||v||_2}$$

where u and v represent GLPI vectors.

All statistical details can be found in the figure legends, figures, and results sections.